Journal of Hazardous Materials 478 (2024) 135540

Contents lists available at ScienceDirect

Journal of Hazardous Materials

journal homepage: www.elsevier.com/locate/jhazmat

Deciphering the spatial organization of fibrotic microenvironment in silica particles-induced pulmonary fibrosis

Liliang Yang [a,1], Xinyan Wei [a,c,1], Piaopiao Sun [a], Jing Wang [a], Xinbei Zhou [a,c], Xinxin Zhang [a], Wei Luo [a,c,d], Yun Zhou [e], Wei Zhang [a], Shencun Fang [b,*], Jie Chao [a,c,d,**]

[a] Jiangsu Provincial Key Laboratory of Critical Care Medicine, Zhongda Hospital, Department of Physiology, School of Medicine, Southeast University, Nanjing, Jiangsu 210009, China
[b] Department of Respiratory Medicine, Nanjing Chest hospital, The Affiliated Brain Hospital of Nanjing Medical University, China
[c] Key Laboratory of Environmental Medicine Engineering, Ministry of Education, School of Public Health, Southeast University, Nanjing, Jiangsu 210009, China
[d] School of Medicine, Xizang Minzu University, Xianyang, Shanxi 712082, China
[e] Department of Health Management, School of Health Science, West Yunnan University of Applied Sciences, Dali, Yunnan 671000 China

HIGHLIGHTS

- The study mapped cell types within and surrounding fibrotic lung regions.
- Silica decreased the number of Inmt fibroblasts but increased that of profibrotic Grem1 fibroblasts.
- Silica induced monocyte-derived alveolar macrophages AM3.
- AM3 promoted Inmt fibroblast differentiation into Grem1 fibroblasts in fibrotic environment.

GRAPHICAL ABSTRACT

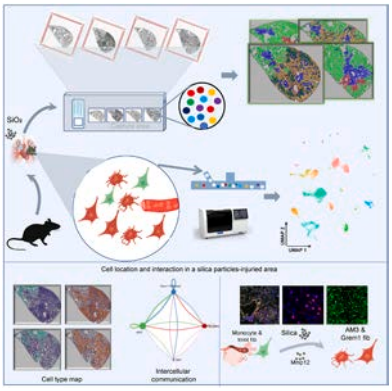

ARTICLE INFO

Keywords:
Crystalline silica
Pulmonary fibrosis
Fibroblast-macrophages homeostasis
INMT

ABSTRACT

Silicosis represents a form of interstitial lung disease induced by the inhalation of silica particles in production environments. A key pathological characteristic of silica-induced pulmonary fibrosis is its localized tissue heterogeneity, which presents significant challenges in analyzing transcriptomic data due to the loss of important spatial context. To address this, we integrate spatial gene expression data with single-cell analyses and achieve a detailed mapping of cell types within and surrounding fibrotic regions, revealing significant shifts in cell populations in normal and diseased states. Additionally, we explore cell interactions within fibrotic zones using ligand-receptor mapping, deepening our understanding of cellular dynamics in these areas. We identify a subset

* Corresponding author.
** Corresponding author at: Jiangsu Provincial Key Laboratory of Critical Care Medicine, Zhongda Hospital, Department of Physiology, School of Medicine, Southeast University, Nanjing, Jiangsu 210009, China.
E-mail addresses: fang1984@aliyun.com (S. Fang), chaojie@seu.edu.cn (J. Chao).
[1] These authors contribute equally to this work.

https://doi.org/10.1016/j.jhazmat.2024.135540
Received 12 May 2024; Received in revised form 24 July 2024; Accepted 14 August 2024
Available online 22 August 2024

of fibroblasts, termed Inmt fibroblasts, that play a suppressive role in the fibrotic microenvironment. Validating our findings through a comprehensive suite of bioinformatics, histological, and cell culture studies highlights the role of monocyte-derived macrophages in shifting Inmt fibroblast populations into profibrotic Grem1 fibroblast, potentially disrupting lung homeostasis in response to external challenges. Hence, the spatially detailed deconvolution offered by our research markedly advances the comprehension of cell dynamics and environmental interactions pivotal in the development of pulmonary fibrosis.

1. Introduction

Silica particles, among the most abundant minerals in nature, are extensively used in agricultural and industrial settings. Their primary entry into the human body occurs through the respiratory tract due to current production methods, posing significant health risks, including silicosis. In 2017, global silicosis cases reached approximately 162,400, with over 23,600 new cases reported [1]. The mortality rate for silicosis remains high, and current pharmaceutical interventions offer limited relief, failing to halt the progression of silica-induced fibrosis. This condition, resulting from prolonged inhalation of free silica particles, is characterized by extensive fibrosis and systemic inflammation in lung tissues. Although the precise mechanisms of silicosis development remain elusive, fibroblasts and macrophages are recognized as key players in pulmonary fibrosis [2].

The pathogenesis of lung fibrosis has traditionally focused on fibroblasts and macrophages, hypothesizing a dysregulated interplay among cellular populations. Yet, the full spectrum of interactions within the fibrotic niche—a specialized microenvironment driving fibrosis—remains underexplored. Extensive literature indicates significant heterogeneity among both fibroblasts and macrophages, with different subtypes potentially playing distinct roles [3]. Under physiological conditions, fibroblast subtypes include lipofibroblasts, airway fibroblasts, alveolar fibroblasts, adventitial fibroblasts, and myofibroblasts [4]. In disease states, novel subtypes such as fibrosis-associated, inflammation-associated, and cancer-associated fibroblasts emerge [3]. Similarly, macrophages include interstitial and tissue-resident macrophages under normal conditions, while other subtypes appear under external stress [5]. The spatial distribution and interactions of these heterogeneous subpopulations in pulmonary fibrosis remain unclear. Elucidating their distribution and interactions is crucial for understanding the pathogenesis of silicosis.

Fibroblasts and macrophages are found in close association in several tissues in the steady state, as demonstrated by Germain et al. using *in vivo* imaging [6]. This association enables reciprocal growth factor signaling between fibroblasts and macrophages. Medzhitov et al. proposed a symbiotic relationship between these cells, suggesting a two-cell circuit where they reciprocally interact and sustain themselves in tissues [7]. This framework suggests that macrophages provide PDGF ligands required for fibroblast survival. The mechanisms by which macrophages influence fibroblast biology have been more extensively addressed in fibrosis than in steady-state tissues. Depletion of macrophages at fibrosis onset limits injury extent, while their loss during fibrotic resolution prolongs fibrosis [8]. Although numerous studies have reported on fibroblast-macrophage interactions in pulmonary fibrosis, the mechanisms of interaction between different subtypes remain poorly understood. Fibroblasts, typically quiescent, become activated in response to pathological stimuli, embarking on proliferation, migration, and extracellular matrix synthesis, contributing to the heterogeneity among lung fibroblasts and underscoring their pivotal role in the fibrotic process [9]. Similarly, the lung harbors diverse macrophage subsets [10–13], whose roles in fibrosis, particularly in response to silica exposure and in conditions like IPF and severe COVID-19, are increasingly recognized yet not fully understood [14–16]. Understanding the interactions and relationships between cellular subpopulations can provide new insights into lung fibrosis treatment.

In silicosis, an excessive buildup of silica particles tends to localize in specific lung regions. Identifying specific lesions is pivotal in understanding the fibrotic process, emphasizing the need to delve into cellular components, signaling pathways, and gene expression profiles at these distinct locations. Previous studies acknowledging spatial heterogeneity often used digital spatial profiling (DSP), which limits the observation of comprehensive gene expression changes and introduces subjective biases in region selection [17]. In contrast, our approach utilized 10x spatial transcriptomics technology [18], preserving the morphological structure of lung sections. This methodology not only allows for a thorough examination of gene expression across the entire tissue section but also mitigates the subjectivity associated with artificial region selection, providing a holistic perspective for measuring and comparing gene expression changes. Simultaneously, we integrated single-cell sequencing data from the same set of spatial transcriptomics samples, offering finer resolution in dissecting cellular compositions and facilitating a comprehensive understanding of spatial interactions among cell types. By employing these advanced technologies, we aim to elucidate the nuanced relationships between different cell types within the spatial context of lung fibrosis, potentially augmenting our understanding of fibrotic pathogenesis and revealing novel therapeutic avenues.

This study utilized advanced technologies, including 10x spatial transcriptomics and single-cell sequencing, to elucidate the spatial distribution and roles of these cells in silicosis. We identified the fibrosis-suppressing Inmt fibroblast subtype and the fibrosis-promoting monocyte-derived alveolar macrophage AM3, highlighting their respective contributions to disease progression. Notably, our findings revealed a decrease in Inmt fibroblasts and an increase in Grem1 fibroblasts in both silica-induced and bleomycin-induced fibrosis, suggesting a conserved mechanism across different fibrotic conditions. Additionally, spatial transcriptomics showed a mutually exclusive distribution pattern between Inmt and Grem1 fibroblasts, as well as between AM3 and AM1 macrophages, emphasizing the spatial heterogeneity and aberrant cell interactions within fibrotic lungs. These findings elucidate the pivotal role of monocyte-derived macrophages and the reduction of Inmt fibroblasts in compromising lung homeostasis in response to environmental challenges. By employing these advanced technologies, we aim to provide a holistic perspective on the cellular dynamics and interactions in lung fibrosis, potentially uncovering novel therapeutic avenues for this debilitating disease.

2. Materials and methods

2.1. Reagents

BSA was purchased from BBI Life Sciences Co (SongJiang District, Shanghai, China). Silica particles (SiO_2), measuring 2–5 μm in diameter, were sourced from Sigma-Aldrich (Product Code S5631, Darmstadt, Germany). The sterilization process for silica involved heating at 200 °C for 16 h and subsequent dilution in sterile Normal Saline (NS) to concentrations of 5 mg/ml for lab assays or 50 mg/ml for animal studies. M-CSF mouse antibodies (catalogue sc-365779) were procured from Santa Cruz Biotechnology (Dallas, Texas, USA), and F4/80 antibodies (catalogue ab100790, sc-26642, and sc-52664) from both Santa Cruz and Abcam (Cambridge, MA, USA). Rabbit anti-CSF1R antibodies (catalogue YT0881) were obtained from Immunoway (Plano, TX, USA).

2.2. Establishment of a mouse model of silicosis

Male C57BL/6 mice were provided by Hangzhou Ziyuan Experimental Animal Co., Ltd. (Hangzhou, China), housed in groups of three to five per cage with a 12-hour light/dark cycle, at a constant temperature of 22 ± 2 °C and 40 ± 10 % humidity, with free access to food and water.

Sigma-Aldrich provided 80 % of the silica particles, with an average diameter of 5 μm (Product Code S5631). Endotoxins were rendered inactive by 16 h of heating at 180°. The final product was then sorted using Stokes' rule. Before the silica samples were utilized in the experiment, they were dissolved in 50 mg/ml of saline solution. Six-week-old male C57BL/6 J mice weighing around 22 g were put to sleep intraperitoneally with 1 % pentobarbital sodium (50 mg/kg in ddH_2O). After the fur was removed and the neck region was cleaned with 75 % alcohol, a 1-cm incision was made to expose the trachea, and 100 μl of either silica or NS (for the control groups) was injected. Following the procedure, the incision was sutured, and the mice were allowed to recuperate while being attentively observed once a day and fasted for six hours before and after the treatment.

2.3. Sirius red and immunofluorescence staining

Lung specimens were fixed in 4 % paraformaldehyde at 4 °C for 24 h, then dehydrated using a sucrose gradient (20 % followed by 30 %) each for a day. After dehydration, specimens were stored at −80 °C until further analysis. Lung sections, 8 μm in thickness, were stained with Sirius red following the Sirius Star Chromosome Kit (Abcam) guidelines. Post staining, sections were rinsed with 1 % acetic acid, and images captured using an EVOS FL Auto 2 microscope (Thermo Fisher Scientific, Waltham, MA, USA) or Olympus VS200 at 20 × magnification.

The immunofluorescence analysis of tissues was performed as described [19]. Following fixation and permeabilization, lung sections were blocked with 10 % normal goat serum and incubated with primary antibodies overnight at 4 °C. Nuclei were stained with DAPI, followed by incubation with fluorescent secondary antibodies.

2.4. Cell culture

ScienCell provided human pulmonary fibroblast-adult (HPF-a) cells, which were then cultured in DMEM enhanced with 100 μg/ml streptomycin, 100 U/ml penicillin,10 % fetal bovine serum, and 2 mM L-GlutaMAX (Gibco). The cells were grown at 37 °C in a CO2 incubator. After stabilizing the cell state, the cells were treated further. Cell density was changed as needed for particular studies. THP-1 cells were cultivated at 37 °C in a CO2 incubator with RPMI1640 supplemented with 10 % FBS, 100 U/ml penicillin and 100 μg/ml streptomycin. For a duration of 24 h, THP-1 cells were treated with 50 nM/well of phorbol acetate (PMA) in order to trigger their differentiation into macrophages.

2.5. Western blot assays

Western blot was used to measure the protein levels in HPF-a cells and mouse lung tissues. A Tanon scanner was used to visualize the results of the experiment. To summarize, 24-well plates containing normal or transfected HPF-a cells were grown, treated with TGF-β1 or conditional culture media, and then twice washed with PBS. Protease inhibitor-containing cell lysis solution (100:1) was used to extract proteins. Similar steps were taken for tissue protein extraction: tissues were crushed, cell lysis buffer with protease inhibitors was added, and the mixture was incubated at −80 °C for the whole night. Following the manufacturer's instructions, the BCA assay was used to determine the extracted protein concentration (Beyotime). After adjusting the concentration, loading buffer was added, and the sample was successfully prepared by boiling it for five minutes at 100 °C to denature the protein. The protein sample was separated using sodium dodecyl sulfate–polyacrylamide gel electrophoresis, then it was transferred to PVDF membranes and blocked for an hour at room temperature using Tris-buffered saline with 5 % skim milk powder in Tween 20 (TBST). After that, the PVDF membrane was incubated with the primary antibody in a chromatography cabinet at 4 °C for at least 16 h. The PVDF membrane was treated with TBST four times the next day, and it was then left to incubate for one hour at room temperature with the secondary antibody. The membrane was treated with a luminous solution and photographed following three further washing.

2.6. Real-time quantitative PCR (qRT-PCR)

To assess the relative mRNA expression of Inmt, qRT-PCR was used. TRIzol reagent (Invitrogen) was used to extract total RNA from mouse lung tissues in accordance with the manufacturer's instructions. The concentration of RNA was then measured with a Thermo Fisher Scientific NanoDrop spectrophotometer. After that, the RNA samples were reverse transcribed into cDNAs and normalized to 400 ng. Using these cDNA samples as templates, cycle threshold (Ct) and ΔCt values were analyzed by qRT-PCR. The Bio-Rad Opticon monitoring software was utilized to quantify ΔΔCt. The endogenous reference (Gapdh) was used to standardize the relative quantification of mRNA expression.

2.7. CCK-8, bromodeoxyuridine (BrdU) labeling and cell migration assays

Cell viability was evaluated using the CCK-8 test in accordance with the manufacturer's instructions (Dojindo, Japan). After the cells were fully treated, 10 μl of CCK-8 solution was added to each well of a 96-well plate, and the mixture was incubated for an hour without light at 37 °C. The absorbance at 450 nm was then determined with a spectrophotometer. By calculating the percentage difference between the experimental group's survival and the control group's, cell viability was ascertained.

Transfected cells were seeded on polylysine-treated glass slides and cultured until reaching optimal density, at which point TGF-β1 was introduced. BrdU reagent (Yeasen, 40204ES60) was dissolved in PBS and added to the medium at a 1:1000 dilution. Following a 4-hour incubation period, cells were fixed with 4 % paraformaldehyde at 4 °C, followed by three PBS washes. Subsequently, denaturation was achieved with 2 N HCl/0.3 % Triton X-100 at room temperature for 30 min, followed by incubation with 0.1 M boric acid buffer (pH 8.0) for 10 min and blocking with goat serum at room temperature for 2 h. The cells were then exposed to a BrdU antibody (SC-32323, Santa Cruz) overnight at 4 °C. After PBS washing, cells were incubated with appropriate fluorescent dye-conjugated secondary antibodies in darkness for 2 h. Following three additional PBS washes, cells were mounted with mounting medium (P36931, Life Technologies). Subsequent imaging of the slides was performed using a fluorescence microscope (Olympus IX70).

An assay for wound healing was used to assess the migratory capacity of cells. After being planted at a density of 1 × 10^5 cells per well in 24-well plates, the cells were kept at 37 °C until 90 % confluency was reached. Next, using a sterile 200-μl pipette tip, a medium-width straight line was gently drawn vertically in the middle of each well. The plates were then cleaned using PBS three times to get rid of any leftover cell debris, and then new standard media was put to each well to encourage cell growth. After that, the cells were stimulated experimentally, and at 0,24, and 48 h after scratching, digital pictures of the wound gaps were taken. Using ImageJ, the distances between the wound edges were measured.

2.8. siRNA-mediated knockdown and construction of stable cell lines

Shanghai Jima Pharmaceutical Co. Ltd. provided the siRNAs. Following the manufacturer's instructions, cell samples were transfected

with 60 nM siRNA duplexes using Lipofectamine 3000 (Thermo Fisher Scientific) diluted in serum-free medium.

Human pulmonary fibroblast-adult (HPF-a) cells were seeded at a density of 3×10^4 cells per well were seeded into a 24-well plate. After 24 h, the culture medium was replaced with lentiviral supernatant (Corues Biotechnology, Nanjing, China). Fluorescence was observed 48 h post lentivirus infection. Stable HPF-a cells overexpressing INMT were obtained through selection with 2 μg/ml puromycin. MMP12-overexpressing THP-1 cells were directly purchased from Corues Biotechnology.

2.9. Spatial and single-cell transcriptomic sequencing

Sample collection, Spatial transcriptomic sequencing (GSE183683) and Single-cell sequencing (GSE183682) were detailed in our previous publication [20].

2.10. RNA scope

RNA scope in situ hybridization followed the ACD protocol (LOT 2011249), with lung tissues prepared identically to those for scRNA sequencing.

2.11. Pseudotime analysis

Pseudotime analysis [21] for selected cell populations was performed using Monocle2; its function is to infer a pseudotime based on the UMAP coordinates. The ordering of cells from a branched process can be represented as a tree.

2.12. Filtering of prognosis-related genes and construction of a gene risk model

In order to create a profibrotic macrophage AM3-related gene risk model, IPF cohorts from three centers were used. First, the prognostic significance of each gene in the expression matrix was evaluated using univariate Cox analysis [22]. All the genes associated with prognosis were identified; we crossed these genes with the 46 AM3 signature genes to identify 21 genes. The "glmnet" package [23] in the R programming language was used to perform least absolute shrinkage and selection operator (LASSO) regression analysis on the 21 genes, and the minimum mean cross-validated error was chosen as λ value so that we could obtain 10 genes. Then, to further screen the AM3 genes associated with prognosis, 10 genes ("NINJ1," "EMP1," "IFITM2," "LHFPL2," "SPP1," "IER3, " "BASP1," "MARCKS," "LGMN," and "PLA2G7") were extracted from the LASSO regression and subsequently enrolled in stepwise Cox regression. This created a risk model that contained four genes: IER3, EMP1, LGMN, and LHFPL2. The Cox coefficients of these four genes were obtained from the multivariate Cox proportional hazards regression analysis. Lastly, the risk score was calculated according to the coefficient and expression value of each gene. Using the median risk score, risk groups were divided into two categories (high-risk and low-risk groups). The prognostic significance of risk groups was evaluated using Kaplan-Meier curves and log-rank tests. After that, the risk score was examined using univariate and multivariate Cox regression to determine whether it was an independent factor affecting the prognosis of IPF patients. The risk group and gender were taken into account as categorical variables in the Cox regression analysis. Age and risk score, however, were regarded as continuous variables.

2.13. Cell type enrichment analysis via MIA

To elucidate the significance of gene expression overlap among spatial transcriptomics (ST) data and specific cell markers, a hypergeometric distribution test was employed. This analysis facilitated the identification of enriched or depleted cell types within the spatial context, contributing to the understanding of cellular dynamics in fibrotic lung tissue.

2.14. scRNA-seq and spatial RNA-seq integration using Cell2location

We used the Cell2location [24] to compute the cell abundance and derive the spatial distribution of cell types in lung tissues.

2.15. Cell-cell communication analysis

The CellChat R toolkit, a cell-to-cell interaction analysis tool that investigates the function of ligand-receptors in particular signaling pathways (https://github.com/sqjin/CellChat), was used to identify cell-cell interaction networks [25]. This analysis involved determining potential interactions between receptors expressed in one cell lineage and ligands expressed in another, or within clusters. For spatial transcriptomic cell communication analysis, we incorporated the spatial locations of cells to infer spatially proximal cell-cell communication.

2.16. Enrichment analysis

Unless otherwise specified, we conducted enrichment analysis using the R package clusterprolifer, focusing on differential genes meeting the criteria of log2 fold change > 1 and adjusted p-value < 0.01.

2.17. Statistics

Statistical analyses were conducted using R (version 4.1.0), with significance set at $P < 0.05$. Unless otherwise specified in the figure legends, comparisons between two groups were assessed using the unpaired Wilcox test with two-tailed P-values. Quantification of staining and blot images was performed using ImageJ software (National Institutes of Health, USA).

3. Results

3.1. Silica particles cause aberrant fibroblast-macrophage interactions in mouse silicosis model

To explore their intricate dynamics and molecular signaling pathways involved in lung fibrosis, we conducted a combined analysis using our previously published single-cell and spatial transcriptomic RNA-seq data [20,26] at acute inflammation (day 7) and collagen deposition (day 56) stages (Fig. 1**A**).

Using CellChat [27] to assess cell-cell communication between fibroblasts and myeloid cells, we found significantly elevated SPP1 and APOE signaling at both 7 and 56 days post SiO_2 treatment, both associated with pulmonary fibrosis (Fig. S1A-B) [28,29]. Additionally, aberrant signals including ICAM, GDF, cholesterol, FGF, and THBS were observed during fibrosis [30–33]. Interestingly, despite some enhanced signals, the SiO_2 group exhibited a decrease in total interactions and interaction strength compared to the NS group at both stages(Fig. 1**B**).

To pinpoint cell populations with significant interaction changes, we compared the number of interactions and interaction strength using differential interaction circle plots (Fig. 1**C**) and heatmaps (Fig. 1**D**). Results revealed a reduction in interactions between lung fibroblasts and macrophages(Fig. 1**C-D**), contrasting with previous literature suggesting enhanced interactions during fibrosis progression [34]. This might be attributed to the spatial and cellular heterogeneity of fibroblasts and macrophages.

3.2. Silica particles decrease the number of Inmt fibroblasts and increase that of pro-fibrotic Grem1 fibroblasts

To investigate the role of fibroblast heterogeneity in pulmonary fibrosis, we analyzed all fibroblasts from the scRNA-seq data and

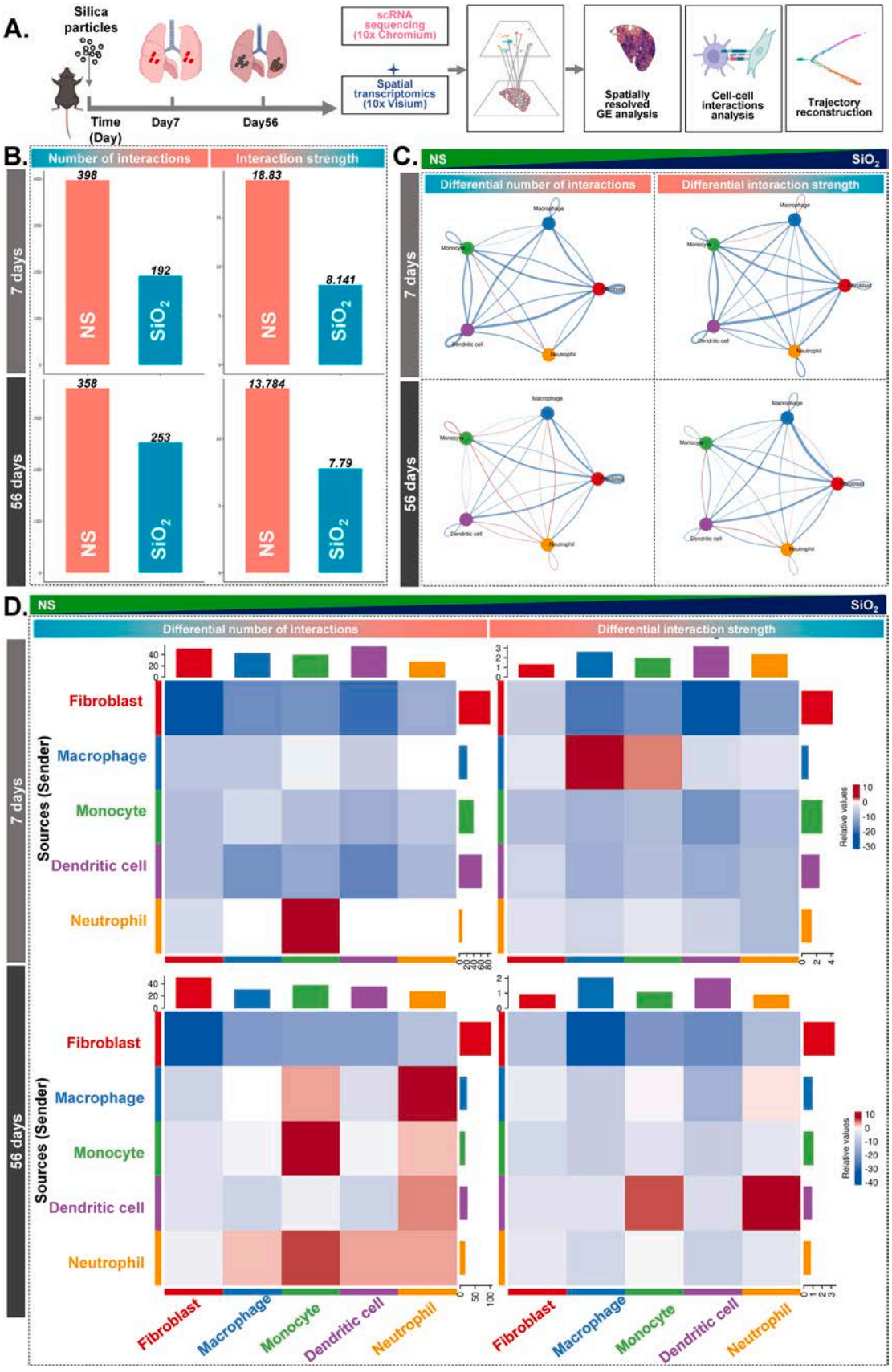

(caption on next page)

Fig. 1. Silica particles decrease fibroblast-macrophage interactions in mouse silicosis model (A) The schematic workflow illustrates the preparation of scRNA-seq and spatial sequencing (ST) libraries, computational analysis, and experimental design. **(B)** The total interactions and interaction strength in the inferred cell-cell communication networks under different biological conditions were computed. The red column represents the normal saline group (NS), while the indigo column represents the silica particles group (SiO_2). **(C)** A circle plot was employed to visualize the differential interactions or interaction strength in the cell-cell communication network between the NS and SiO_2 groups. Red (or blue) colored edges indicate increased (or decreased) signaling in the SiO_2 group compared to the NS group. **(D)** CellChat presents the differential interactions or interaction strength in greater detail using a heatmap. The top colored bar plot shows the sum of each column of absolute values displayed in the heatmap (incoming signaling), while the right colored bar plot shows the sum of each row of absolute values (outgoing signaling). In the colorbar, red (or blue) denotes increased (or decreased) signaling in the SiO_2 group compared to the NS group.

identified 5 fibroblast subclusters: Inmt fibroblast, Grem1 fibroblast, universal fibroblast, Hhip fibroblast, and Myofibroblast (Fig. 2**A-B;** Table. S1**).** Inmt fibroblasts, characterized by high expression of Inmt, decreased after silica treatment, whereas Grem1 fibroblasts, known for their inflammatory-proliferative properties [26], increased significantly (Fig. 2**C and S2A)**.

Inmt fibroblasts exhibited a high expression of alveolus function-associated genes and potential responsiveness to toxic substances (Fig. 2**D)**. Grem1 fibroblasts, on the other hand, upregulated collagen-related genes such as Tnc and Col7a1 and showed increased Runx1 expression(Fig. 2**B)**, implicated in lung fibrosis development [35]. Progeny analysis [36] revealed high TGFb signaling activity in Grem1 fibroblasts and low activity in Inmt fibroblasts (Fig. 2**E)**. Consistently, Gene Ontology (GO) analysis indicated that Inmt fibroblasts are involved in cellular detoxification and alveolus function, whereas Grem1 fibroblasts are enriched in inflammation and fibrogenesis-related terms (Fig. 2**F)**.

Western blot, qPCR and immunofluoresence analyses confirmed the decreased expression of Inmt in lung tissues post-silica treatment (Fig. 2**G-I and S2B).** Spatial transcriptomics using Cell2location [24] showed that Inmt fibroblasts predominated in uninjured lung tissues, while Grem1 fibroblasts localized to injury sites (Fig. 2**J)**. Trajectory analysis by monocle2 [37] indicated that Grem1 fibroblasts might derive from Inmt fibroblasts (Fig. 2**K)**.

To delve deeper into Inmt's function, we performed GO analysis of Inmt fibroblast marker genes, revealing roles in fibrosis, such as cell-matrix adhesion and extracellular matrix organization (Fig. 3**A).** INMT knockdown in human pulmonary fibroblast-adult (HPF-a) cells enhanced fibroblast viability, while INMT overexpression had no significant effect compared to controls (Fig. S2C**-D)**. INMT knockdown also increased BrdU positive fibroblast numbers induced by TGF-β1 (Fig. 3**B-C)**, confirming the role of INMT in cell proliferation [38]. Furthermore, INMT knockdown significantly enhanced fibroblast migration (Fig. 3**D–E)** and activation markers (Fig. 3**F-I)**. Conversely, INMT overexpression suppressed TGF-β1-induced proliferation (Fig. 3**J-K)**, migration (Fig. 3**L-M)**. and fibroblast activation markers (Fig. 3**N-Q),** confirming INMT's inhibitory role in these fibrosis-related phenotypes.

We also analyzed a previously published dataset on bleomycin-induced lung fibrosis [39] and identified eight fibroblast subtypes, including Inmt and Grem1 fibroblasts (Fig. S2E). Consistent with our findings in the silica model, Inmt fibroblasts decreased while Grem1 fibroblasts increased after bleomycin treatment (Fig. S2F). Inmt fibroblasts were associated with alveolus function and response to toxic substances, while Grem1 fibroblasts were linked to immune cell chemotaxis and fibroblast migration (Fig. S2G**-H)**. Progeny analysis [36] showed high TGFβ signaling in Grem1 fibroblasts and low TGFβ signaling in Inmt fibroblasts in the bleomycin model (Fig. S2I).

3.3. Silica particles induce monocyte-derived alveolar macrophage

Macrophage subclustering revealed two main groups: tissue-resident interstitial macrophages (IMs) and alveolar macrophages (AMs) (Fig. 4**A-B**). IMs were identified through the expression of C1qa, C1qb, and C1qc (Fig. 4**B**). Both AMs and IMs expressed Lyz2, Cd68, and Adgre1, while Marco and Il18 were exclusively present in AMs (Fig. S3A).

Among the AMs, three distinct subtypes were identified: AM1, AM2, and AM3. AM1 macrophages, associated with cell maturity and tissue homeostasis (Ptbp3, Cib2, and Pparg), were predominantly found in the lungs of control mice, whereas AM3 macrophages, with a pro-fibrotic phenotype (Gpnmb, Vegfa, Spp1, Ctss, Lilrb4a, and Litaf), predominated in silica-treated mice (Fig. 4**C and** Fig. S3B**;** Table. S2**).** Monocle analysis indicated that AM3 macrophages originated from monocytes (Fig. 4**D**), a finding further confirmed by re-analysis of $Ccr2^{-/-}$ mice data [40] (Fig. S3C**-G;** Table. S3**).**

To elucidate the connection between AM3 and lung fibrosis, we utilized the Comparative Toxicogenomics Database [41] to investigate the expression profiles of 947 genes linked to pulmonary fibrosis. Comparative analysis identified 117 pulmonary fibrosis-related genes expressed in AM3 macrophages, including pro-fibrotic genes distinct from those in AM1 and AM2. While AM1 macrophages expressed "generic" genes associated with lipid and tissue homeostasis, AM3 macrophages were enriched with pro-fibrotic genes associated with fibroblast activation (Fig. 4**E-F;** Table. S4**-5).** Immunofluorescence staining and Cell2location analysis showed that AM3 macrophages localized to damaged lung regions, supporting their role in fibrosis progression (Fig. 4**G-H).** In contrast, AM1 macrophages were more evenly distributed in normal group and not specifically associated with fibrotic areas.

In the bleomycin-induced lung fibrosis model [42], we also identified three subclusters (AM1, AM2, and AM3) within the macrophage population (Fig. S3G**-J;**Table. S6). Similar to our silica-induced fibrosis model, AM1 and AM2 were comprised of cells from both the bleomycin-treated and saline-treated groups, while AM3 macrophages were primarily found in the bleomycin-treated group (Fig. S3J**)**. Comparative analysis revealed 141 pulmonary fibrosis-related genes in the bleomycin dataset, with 85 genes more frequently expressed in AM3, including Mmp12, Timp2, Mmp14, Spp1, Pdgfa, Fn1, Itgam, and Gpnmb (Fig. S3K **and** Table. S7). A pro-fibrotic AM cluster was also observed in lung tissue samples from individuals with IPF [43], sharing commonalities with the AM3 in mice with silica-induced and bleomycin-induced pulmonary fibrosis, evidenced by 46 shared genes such as Gpnmb, Spp1, and Itgam (Fig. S3l **and Table. S 7)**.

To determine the clinical relevance of pro-fibrotic AM3, we analyzed gene expression data (GSE70867) from IPF patients. Adjusting for sex and age, 2027 genes were predictive of mortality (Table. S8**),** with 21 out of 46 AM3 signature genes included. LASSO regression (Fig. S4A**)** identified 10 significant genes, refined to 4 (IER3, EMP1, LGMN, LHFPL2) by Cox regression for a risk score. The risk score derived from AM3 feature genes was an independent factor affecting IPF prognosis (Fig. S4B**-4 C;**Table. S9**)**.

3.4. Maintaining AM3 in fibrotic niches requires the Csf1/Csf1r signal

To investigate the survival support mechanisms of monocyte-derived AM3, we reviewed existing literature and found that Csf1/Csf1r signaling is critical for the maintenance of AMs in mutant mice [44,45]. When mice were exposed to silica or bleomycin, Csf1r was elevated in the AM3 cluster (Fig. 5**A and** Fig. S5A**).** Therefore, we explored the cells expressing Csf1r ligands Csf1 and Il34, and identified that alveolar type II cells and fibroblasts expressed Il34, whereas fibroblasts, endothelial, epithelial cells, neutrophils and AM3 expressed Csf1 (Fig. S5B**)**. Our analysis revealed that approximately 20 % of AM3 macrophages expressed Csf1 in both murine and human datasets (Fig. 5**A and B and**

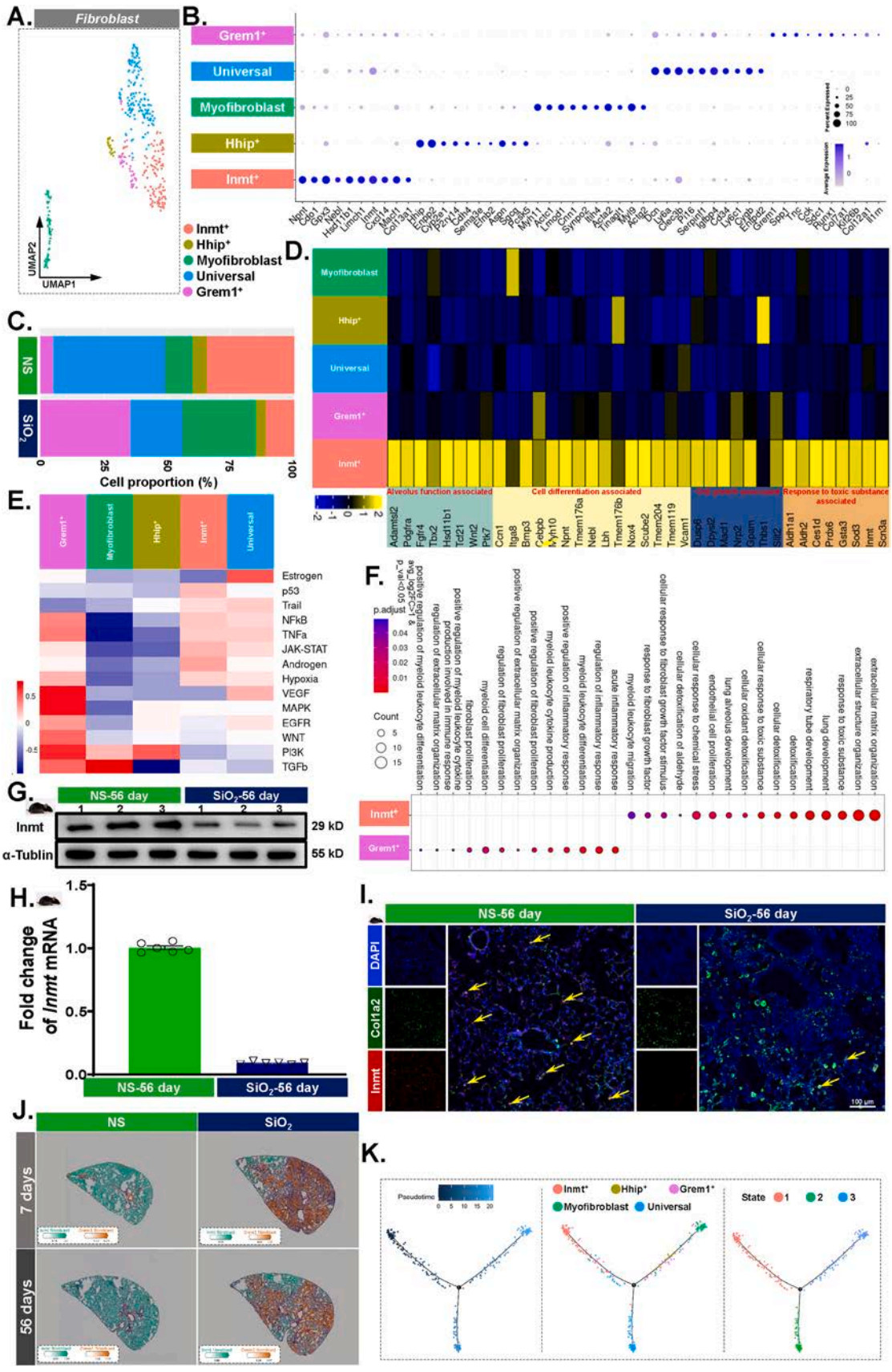

(caption on next page)

Fig. 2. Variability of fibroblast states. (A) UMAP plot shows fibroblasts subsets. **(B)** UMAP plot shows fibroblasts subsets. **(C)** Bar plot shows the composition of fibroblast subclusters in cells from silica- and saline-exposed animals. To better present and interpret the results, we combined NS_7 and NS_56 into a single NS group, and SiO_2_7 and SiO_2_56 into a single SiO_2 group for the cell proportion analysis. All the missing time points are included in the Fig. S2A. **(D)** Heatmap shows the highly expressed genes in Inmt fibroblast. **(E)** Progeny analysis shows the pathway activity across fibroblast subsets. **(F)** Dotplot shows GO enrichment terms of Inmt and Grem1 fibroblast markers. **(G)** Western blot probes the protein expression of Inmt after silica treatment. **(H)** q-PCR probes the mRNA expression of Inmt after silica treatment. **(I)** Immunofluorescence shows the expression of Inmt protein in normal and silica-treated condition. Col1a2 stains for fibroblasts and DAPI stains for cell nuclei.Vimentin-stained fibroblast results are in Fig. S2B. **(J)** Using cell abundance score calculated by Cell2location visualizes Inmt and Grem1 fibroblasts in the spatial slides. **(K)** Monocle2 pseudotime trajectory shows differentiation relationships between distinct fibroblasts subpopulations.

Fig. S5C**)**, which was corroborated through bulk RNA sequencing of murine models and examination of human lung tissue samples [46] **(**Fig. S5D**)**. In a human IPF dataset [47] (Fig. S5E), we identified the AM3 cluster **(**Fig. 5**C-D)** and observed increased CSF1R expression in IPF patients, implicating the CSF1/CSF1R pathway in the disease process **(**Fig. 5**E)**. CellChat analysis [25] indicates that AM3 macrophages produce an autocrine CSF signal promoting their persistence **(**Fig. 5**F).** Immunofluorescence and Sirius red staining analysis confirmed the presence of $Csf1^+$ and $Csf1r^+$ macrophages in fibrotic areas **(**Fig. 5**G).**

3.5. Silica particles induce spatial molecular variation in silicosis mouse model

To elucidate spatial signature changes post-silica exposure, we performed detailed spatial transcriptomics analysis. Integration and clustering of spatial transcriptomic data revealed nine unique clusters (Fig. 6**A, leftmost panel)**. UMAP plot showed aggregation of NS groups, while SiO_2 groups separated significantly, indicating gene alterations induced by silica (Fig. 6**A, middle panel**). Spatially, clusters 6 and 4 were localized around bronchial and blood vessels, while clusters 1 and 3 were situated in lung injury areas caused by silica particles (highlighted in yellow circles) (Fig. 6**B, column 1 and 2**). TGF-β signaling pathway enhancement was noted in injured areas (highlighted in red circles) (Fig. 6**B, column 3**). Cell2location [24] analysis showed a reduction of Inmt fibroblasts (Fig. 6**B, column 4**) and an increase of AM3 macrophages and Grem1 fibroblasts in injured areas (Fig. 6**B, columns 5 and 6**), suggesting their spatial involvement in lung fibrosis.

We categorized the nine clusters into five major regions: bronchial, vascular, interstitial, fibrogenic, and inflammatory zones**(**Fig. 6**A, rightmost panel).** These regions corresponded to anatomical structures and pathological characteristics from H&E staining **(**Fig. 6**B, columns 1 and 2;** Fig. 6**C)**, which is consistent with the enrichment results obtained using region-specific markers **(**Fig. 6**D;** Fig. S6A**)**. Furthermore, using *Fmos* and *Pln* as markers, we validated the presence of bronchial and vascular zones**(**Fig. 6**E).** Collectively, the spatial transcriptomics analysis revealed unique gene profiles corresponding to distinct anatomical and injury regions in fibrotic mouse lungs.

3.6. Silica particles sculpt a fibrotic microenvironment characterized by the concurrent presence of AM3 macrophages and Grem1 fibroblasts, while devoid of AM1 macrophages and Inmt fibroblasts

To elucidate spatial dynamics among fibroblasts and macrophages, we applied Multimodal Integration Analysis (MIA) [48] to integrate single-cell data and spatial transcriptomics data. AM3 macrophages were significantly enriched within fibrogenic zones, inversely correlated with the depletion of Inmt fibroblasts **(**Fig. 7**A)**, a finding echoed by our Cell2location analysis (Fig. 7**B, columns 1–3 and 5;** Fig. S7A**-D**).

We visualized the spatial distribution of AM1, AM3 macrophages, Inmt, and Grem1 fibroblasts using Cell2location, showing increased AM3 macrophages and decreased Inmt fibroblasts in inflammatory and fibrogenic zones post-silica-induced lung injury (Fig. 7**B, column 2 and 3**). This suggests that AM3 macrophages likely facilitate the differentiation of Inmt fibroblasts into Grem1 fibroblasts, as evidenced by the concurrent increase in Grem1 fibroblasts in these same areas (Fig. 7**B, column 4).** Further, AM3 macrophages and Inmt fibroblasts showed mutually exclusive enrichment post-injury **(**Fig. 7**B, column 5)**, with a negative correlation in their signature scores within fibrogenic zones **(**Fig. 7**C, upper panel)**. Conversely, AM3 macrophages and Grem1 fibroblasts co-localized **(**Fig. 7**B, column 6)**, with a positive correlation in their signature scores **(**Fig. 7**C, lower panel)**, suggesting AM3's role in facilitating this cellular transition. Finally, our quantified analysis confirm the spatial distribution of different cell populations**(**Fig. 7**D and** Fig. S7E-H**)**.

To further elucidate AM3 and Inmt fibroblasts' roles in pulmonary fibrosis, we conducted differential analysis using spot-level gene expression after excluding bronchial and vascular zones. Regions with AM3 macrophages but lacking Inmt fibroblasts (**identified as red spots in** Fig. 7**E**) exhibited heightened inflammation, TGF-β production, and fibroblast activation pathways (Fig. 7**F).** Conversely, regions with Inmt fibroblasts without AM3 macrophages (**depicted as grey spots in** Fig. 7**E**) displayed increased tissue homeostasis and endothelial proliferation (Fig. 7**F**). Inmt fibroblasts showed a spatial preference for direct contact with AT2 cells **(**Fig. 7**G)**, maintaining tissue homeostasis [49], while AM3 macrophages did not show the preference.

To validate the interaction between AM3 and Inmt fibroblasts, we performed separate cell interaction analyses for the SiO_2 and NS groups of spatial transcriptomics data, focusing on AM3, AM1, Grem1 and Inmt fibroblasts. The results revealed specific interactions between AM3 and Inmt fibroblasts in the SiO_2 group, with stronger interactions between AM3 and Grem1 fibroblasts (Fig. 8**A**). We speculate that AM3 stimulates Inmt fibroblasts to transform into Grem1 fibroblasts.

To identify key molecule capable of mimicking AM3 for *in vitro* simulation, we conducted a protein-protein interaction (PPI) analysis on fibrosis-related genes in AM3 and identified MMP12 as a key molecule (Fig.8**B-C**). Hence, to investigate the activation effect of AM3 on fibroblasts, we overexpressed MMP12 in THP-1 cells, followed by PMA induction to differentiate them into macrophages, thereby simulating AM3 **(**Fig.8**D)**. Relative to the control conditioned medium (NC-CM), conditioned medium from MMP12-overexpressing macrophages (AM3 mimic-CM) heightened the expression of fibroblast activation markers and Grem1, while reducing Inmt expression **(**Fig.8**E;** Fig. S8A**-E)**. Nevertheless, INMT overexpression in fibroblasts counteracted this effect **(**Fig.8**E;** Fig. S8A**-E)**, confirming AM3 macrophages' role in facilitating Inmt fibroblasts' transition to pro-fibrotic Grem1 fibroblasts **(**Fig. 8**F)**.

4. Discussion

In this study, we explored the heterogeneity in pathological alterations within tissues of lung fibrosis, attributing the observed variability to differential timing and spatial distribution of pathophysiological events. Employing spatial transcriptomics, we achieved a nuanced understanding of the microenvironmental dynamics and intercellular communications within fibrotic regions of the lung. This advanced approach facilitated the identification of distinctive gene expression patterns, elucidating alterations in cell populations pivotal for homeostasis and pathology.

4.1. Fibroblast subtypes and spatial distribution

Our results revealed that Inmt fibroblasts are associated with cellular detoxification and alveolus function, while Grem1 fibroblasts are enriched in inflammation and fibrogenesis-related terms. Spatially, Inmt

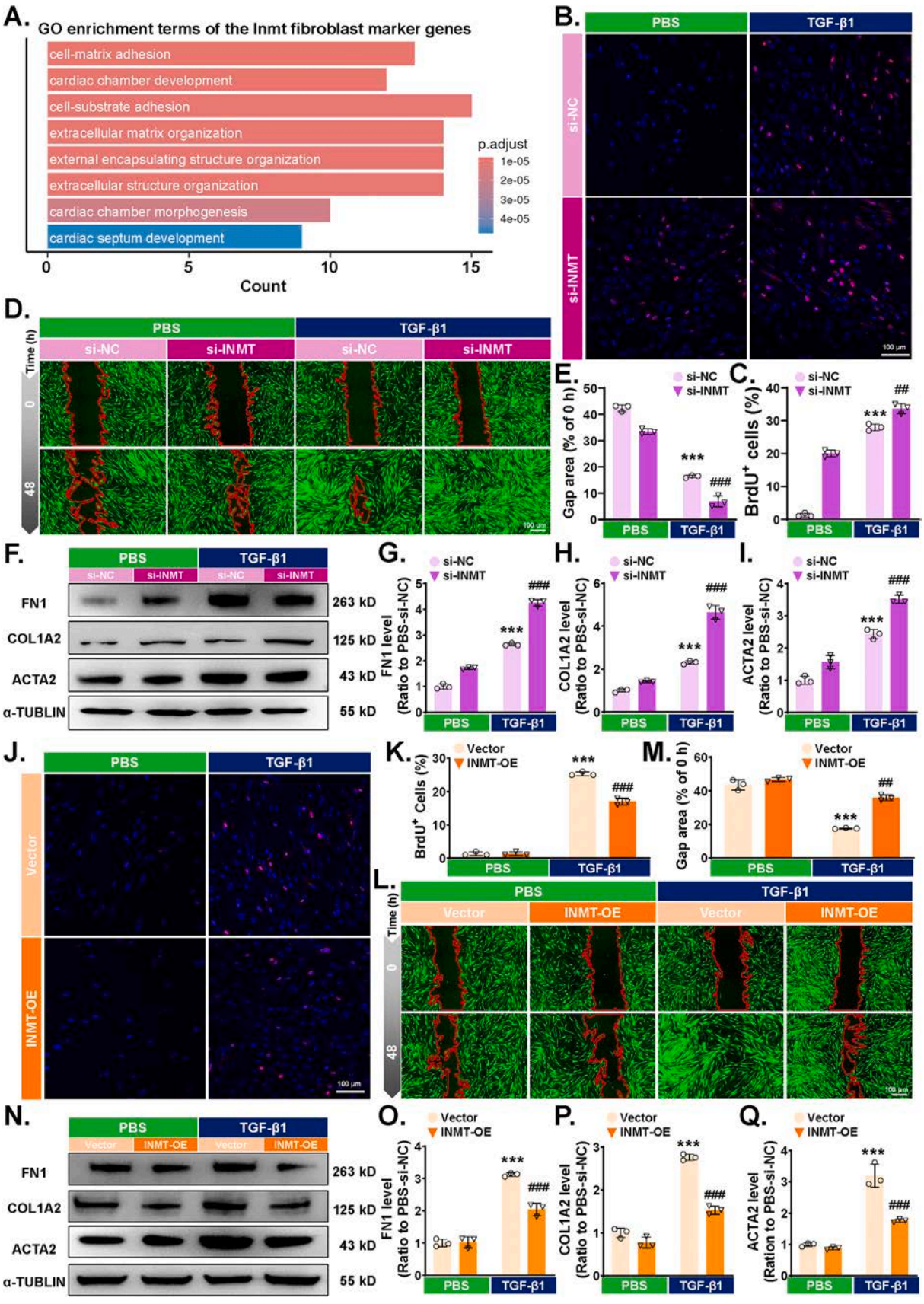

(caption on next page)

Fig. 3. INMT is involved fibroblast dysfunction in lung fibrosis. (A) Gene Ontology (GO) analysis was conducted on marker genes of Inmt fibroblasts. **(B-C)** BrdU incorporation was examined via cellular immunofluorescence. Merged immunofluorescence images of BrdU (red) and DAPI (blue) reveal that INMT downregulation enhances cell proliferation. **(D-E)** The wound-healing assay was utilized to evaluate the influence of INMT downregulation on the migration of human pulmonary fibroblast HPF-a. **(F-I)** Western blotting (WB) was performed to investigate the effects of INMT knockdown on activation markers FN1, Collagen 1, and ACTA2 in human pulmonary fibroblast HPF-a. **(J-K)** BrdU incorporation examined the effects of INMT overexpression on TGF-β1-induced fibroblast proliferation. **(L-M)** The wound-healing assay was utilized to evaluate the influence of INMT overexpression on the migration of human pulmonary fibroblasts. **(O-Q)** WB was performed to investigate the effects of INMT overexpression on activation markers FN1, Collagen 1, and ACTA2 in HPF-a fibroblasts. All the data are presented as the mean ± SD, $n = 3$. Asterisks (*) denote comparisons with the PBS-si-NC or PBS-Vector group: *P < 0.05, * *P < 0.01, * **P < 0.001. Hash symbols (#) denote comparisons with the TGF-β1-si-NC or TGF-β1-Vector group: #P < 0.05, ##P < 0.01, ###P < 0.001.

fibroblasts and Grem1 fibroblasts exhibit mutually exclusive distribution patterns. Previous studies have also explored the spatial heterogeneity of fibroblasts. For instance, Schiller et al. found that Sfrp1 intermediate fibroblasts are commonly located adjacent to fibroblastic foci in IPF patients but are rarely present in areas of severe fibrosis marked by fibroblastic foci [50]. Similarly, in colorectal cancer (CRC) research, FAP fibroblasts were found to be prevalent in the desmoplastic structures of CRC cancer tissues, promoting cancer progression [51]. These findings highlight that fibroblasts exhibit not only identity heterogeneity but also spatial heterogeneity, which plays a crucial role in disease progression and warrants further investigation.

The decrease in the frequency of Inmt fibroblasts and the increase in that of Grem1 fibroblasts were observed in both silica-induced and bleomycin-induced fibrosis. This suggests that Inmt fibroblasts might serve as a reservoir, being induced into other types upon external stimuli, with the Grem1 subtype promoting pulmonary fibrosis. Whether Inmt fibroblasts can differentiate into other subtypes besides Grem1 remains to be explored. Maintaining the homeostatic function of Inmt fibroblasts and reducing the pro-fibrotic capacity of Grem1 fibroblasts could offer therapeutic opportunities for pulmonary fibrosis. Further research is needed to determine the relationship between Inmt fibroblasts and known subtypes like lipofibroblasts [3] or lung specialized fibroblasts (*NPNT*$^{+}$ Alveolar) [52].

4.2. Role of Inmt and INMT in fibroblasts

Our study suggests that Inmt inhibits fibroblast proliferation, activation, and migration, similar to its role in prostate cancer [53]. However, the roles of Inmt (in mice) and INMT (in humans) might be distinct, complicating the comparison of *in vitro* experiments from Fig. 3 with scRNA-seq data from mice. Nevertheless, Inmt expression is decreased in both mouse and human fibroblasts when comparing normal and fibrotic groups [54], suggesting a conserved role across species. Although the fibroblast composition is more complex in human lung tissue, we still found that INMT is predominantly expressed in the specialized lung fibroblast (NPNT^{+} alveolar) subpopulation [52]. Further research is needed to determine whether Inmt fibroblasts in human lungs function similarly to those in mice.

4.3. Macrophage subtypes and spatial distribution

Traditionally, macrophages are classified into M1 and M2 types [55]. However, our analysis of single-cell data from silica-induced fibrosis revealed that alveolar macrophages (AMs) could be divided into AM1, AM2, and AM3, similar to findings in asbestos-induced fibrosis [56]. AM1 macrophages in both studies are associated with homeostatic functions (Ear1 and Fabp1), AM2 macrophages with inflammation (S100a1 and Ctsk), and AM3 macrophages with fibrosis (Fn1 and Spp1). Additionally, we discovered that the pro-fibrotic AM3 subtype appears not only in silica-induced pulmonary fibrosis but also in asbestos-induced [56] and bleomycin-induced pulmonary fibrosis [57], as well as in the lungs of critically ill COVID-19 patients with fibrosis (CD163/LGMN-MΦ) [58]. Our analysis found that AM3 could derive from monocytes, suggesting that macrophages achieve generalized functions and specialization via a lineage-wide core transcriptomic signature and tissue-specific programming influenced by various microenvironmental cues [59,60]. Our study also found that AMs exhibit spatial heterogeneity. Spatial transcriptomics indicated a mutually exclusive distribution pattern between AM1 and AM3. AM1 macrophages primarily localize in undamaged alveolar regions, whereas AM3 macrophages are predominantly found in inflamed and fibrotic areas. Similar disease-dependent spatial distributions of macrophage subtypes have been observed in other conditions [51,61,62]. Intervening in specific macrophage subtypes at particular sites could enhance our understanding of disease mechanisms.

4.4. Monocyte-derived alveolar macrophage AM3

Single-cell RNA sequencing reveals variability within cell populations that arises during illness [63–65]. We demonstrated how data from diseased individuals and animal models can be combined to identify shared processes in disease pathogenesis. Based on our scRNA-seq analysis, AM3 emerged during pulmonary fibrosis [47,57]. Immunofluorescence further confirmed the presence of AM3. Interestingly, AM3 were characterized by increased expression of Spp1, Marcks, Ctsb, Mafb, Gpnmb, Itgam, Csf1r, and Mmp14. Some of these genes were associated with fibrosis [66–72]. Of note, AM3-related four-gene signature (LGMN, IER3, EMP1, and LHFPL2) predicts survival in IPF patients. We propose that depletion of the monocyte-derived alveolar macrophage AM3 might slow the progression of pulmonary fibrosis. Disruption of the Csf1/Csf1r signal of AM3 might help in this regard.

4.5. Fibroblast-macrophage interactions

The role of macrophages in promoting fibroblast activation and differentiation in fibrosis is well established, but the interactions between different macrophage and fibroblast subtypes remain unclear. Our analysis revealed an increase in AM3 macrophages and Grem1 fibroblasts, alongside a reduction in Inmt fibroblasts and AM1 macrophages in fibrotic lung areas. We validated that monocyte-derived AM3 could decrease Inmt fibroblast populations and increase Grem1 fibroblast numbers, potentially disrupting lung homeostasis. AM3 macrophages might drive the differentiation of Inmt fibroblasts into Grem1 fibroblasts. Our *in vitro* experiments showed that AM3 macrophage supernatant decreases Inmt levels and increases Grem1 levels in fibroblasts. However, this does not exclude that fibroblasts might also affect AM3 macrophages. Recent studies show that stromal cells like fibroblasts can regulate immune cell functions, affecting lung fibrosis [73,74]. The immuno-regulatory function of fibroblasts in silicosis via CXCL14 [75] provides a new perspective for understanding fibrosis. Understanding the bidirectional interactions between fibroblasts and macrophages may be crucial for developing effective therapeutic strategies for fibrotic diseases. Our research implies that targeting the AM3 and its signaling pathways could promote the homeostatic function of Inmt fibroblasts and reduce pulmonary fibrosis. Future studies should aim to identify the key regulatory factors of these interactions and explore their potential as therapeutic targets.

4.6. Spatial transcriptomics and disease progression

Bulk RNA-seq lacks spatial information about gene expression, and changes in gene expression at the site of injury onset may be critical in

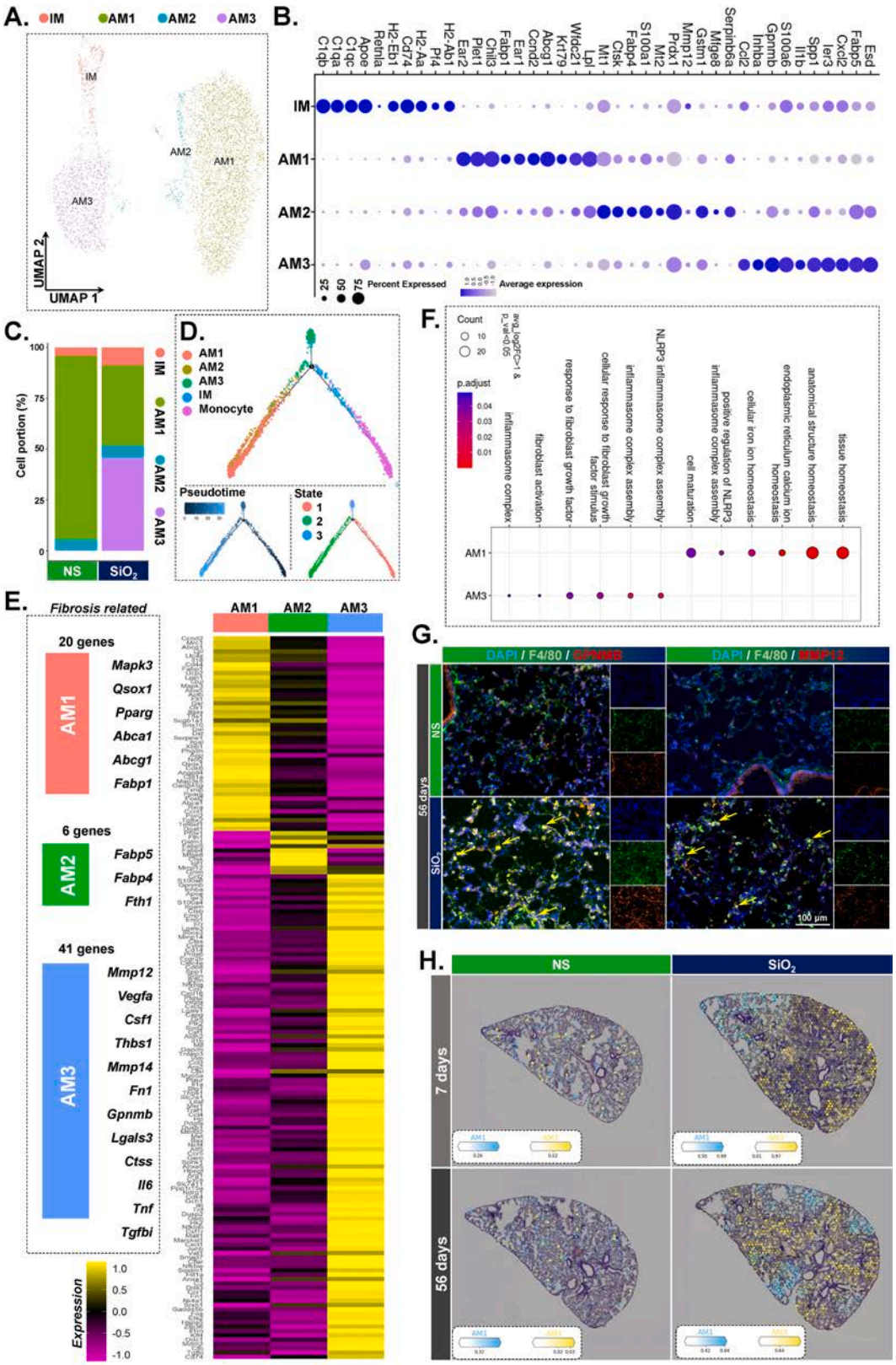

Fig. 4. Alveolar macrophage cell heterogeneity. (A) UMAP plot shows macrophage subsets. **(B)** Dot plot demonstrates the gene expression of macrophages subpopulations in our dataset. **(C)** Bar plot shows the composition of macrophage subclusters in cells from silica- and saline-exposed animals. To better present and interpret the results, we combined NS_7 and NS_56 into a single NS group, and SiO_2_7 and SiO_2_56 into a single SiO_2 group for the cell proportion analysis. All the missing time points are included in the Fig. S2B. **(D)** Monocle2 pseudotime trajectory shows differentiation relationships between distinct myeloid subpopulations. **(E)** Heatmap shows the genes related to fibrosis. (F) Dotplot shows GO enrichment terms of AM1 and AM3 macrohpages markers. (G) Immunofluorescence show the macrophages expressed F4/80, Mmp12 and Gpnmb before and after silica treatment. **(H)** Using cell abundance score calculated by Cell2location visualizes AM1 and AM3 macrophages in the spatial slides.

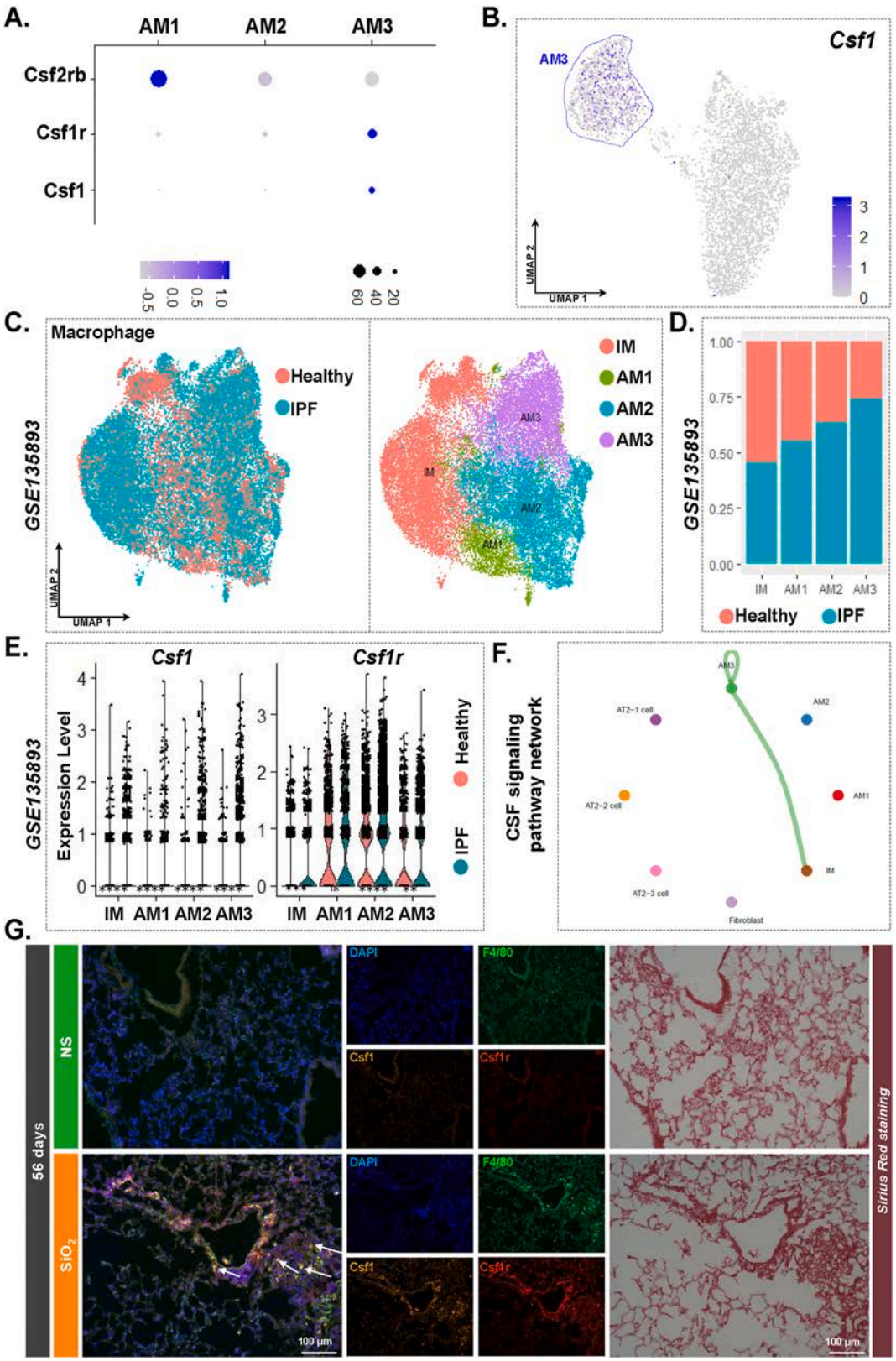

Fig. 5. Autocrine signaling of Csf1/Csf1r in monocyte-derived alveolar macrophages (AM3) maintenance within fibrosis. **(A)** Dotplot showcases the expression of Csf2rb, Csf1r, and Csf1 in AM subclusters in response to silica and saline exposures. **(B)** Feature plot highlights the specific expression of Csf1 in the AM3 subset post-silica treatment. **(C)** UMAP and **(D)** Bar plot demonstrating composition of the macrophage subclusters in human IPF patients or donors from GSE135893. **(E)** Violin plots representing heterogeneity in expression of CSF1 and CSF1R in macrophage subclusters from normal and fibrotic lungs (GSE135893). * ** *: $p \leq 0.0001$, * ** : $p \leq 0.001$, * *: $p \leq 0.01$, * : $p \leq 0.05$, ns: $p > 0.05$. Two-sided Wilcoxon test. (F) Cellchat analysis indicated autocrine CSF signal pathway within AM3. (G) Immunofluorescence and Sirius Red staining on the serial slides showcase Csf1 and Csf1r expression in AMs within silica-induced fibrosis, with white arrows indicating Csf1 and Csf1r positive macrophages.

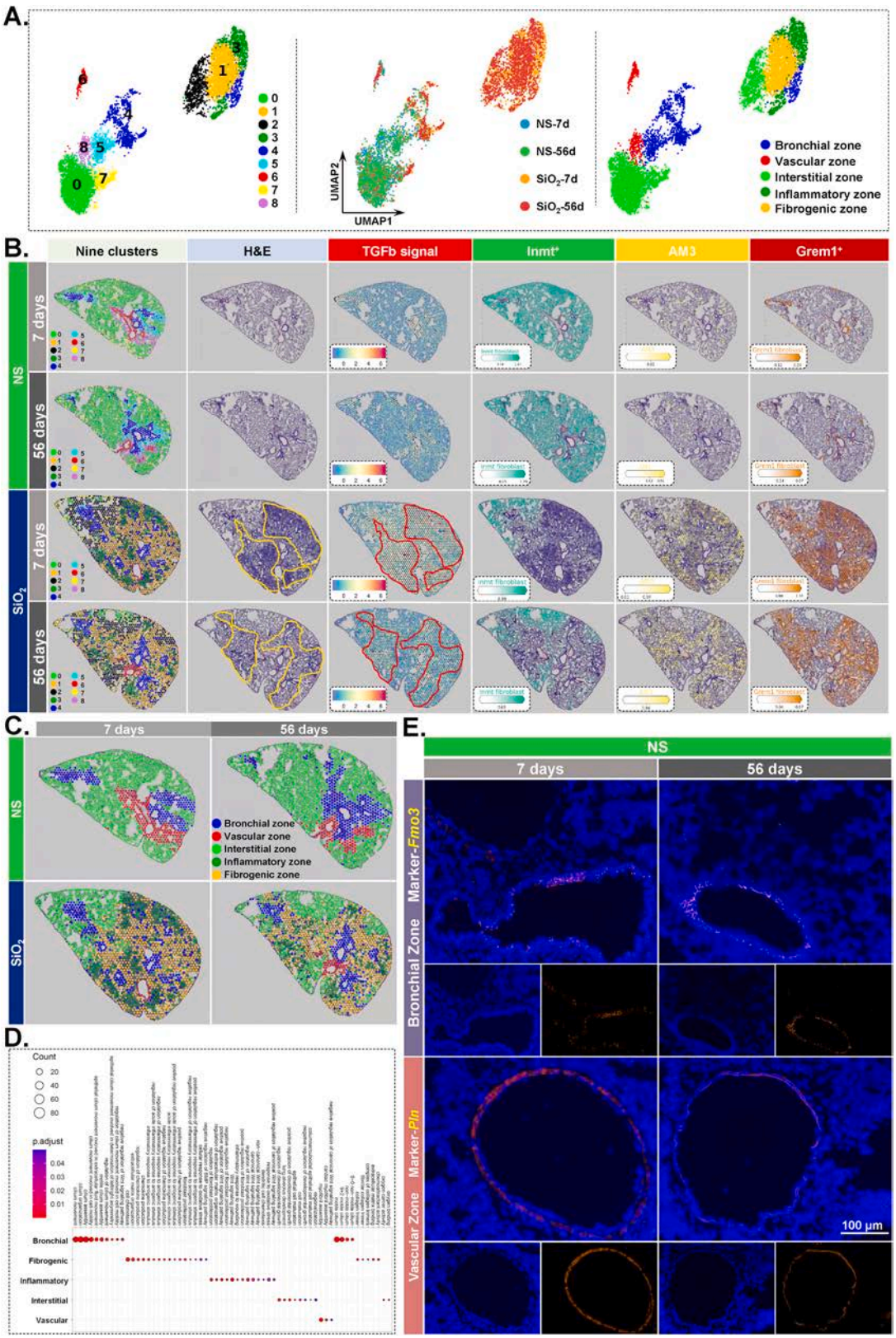

Fig. 6. Silica particles induce spatial molecular variation in silicosis mouse model. (A) The distribution and unbiased clustering of the four spatial sequencing (ST) samples was presented using UMAP in the leftmost and middle panel. **(B)** The first column shows the unbiased clusterings of spatial slides in middle panel from Fig. 6A; the second column shows hematoxylin and eosin (H&E) staining of tissue sections in ST samples (yellow circle indicates the injured tissue); the third column shows the TGFb signal score calculated by Progeny (red circle indicates the injured tissue); and the others show the cell abundance of Inmt fibroblasts and AM3 macrophages as well as Grem1 macrophages. **(C)** ST slides were classified into 5 regions based on anatomical structure and pathological characteristics revealed by HE staining. **(D)** GO terms of genes significantly enriched in each regions of Fig. 6C. **(E)** RNASCOPE in NS_7d and NS_56d groups for bronchial zone (*Fmo3*) and vascular zone (*P*ln).

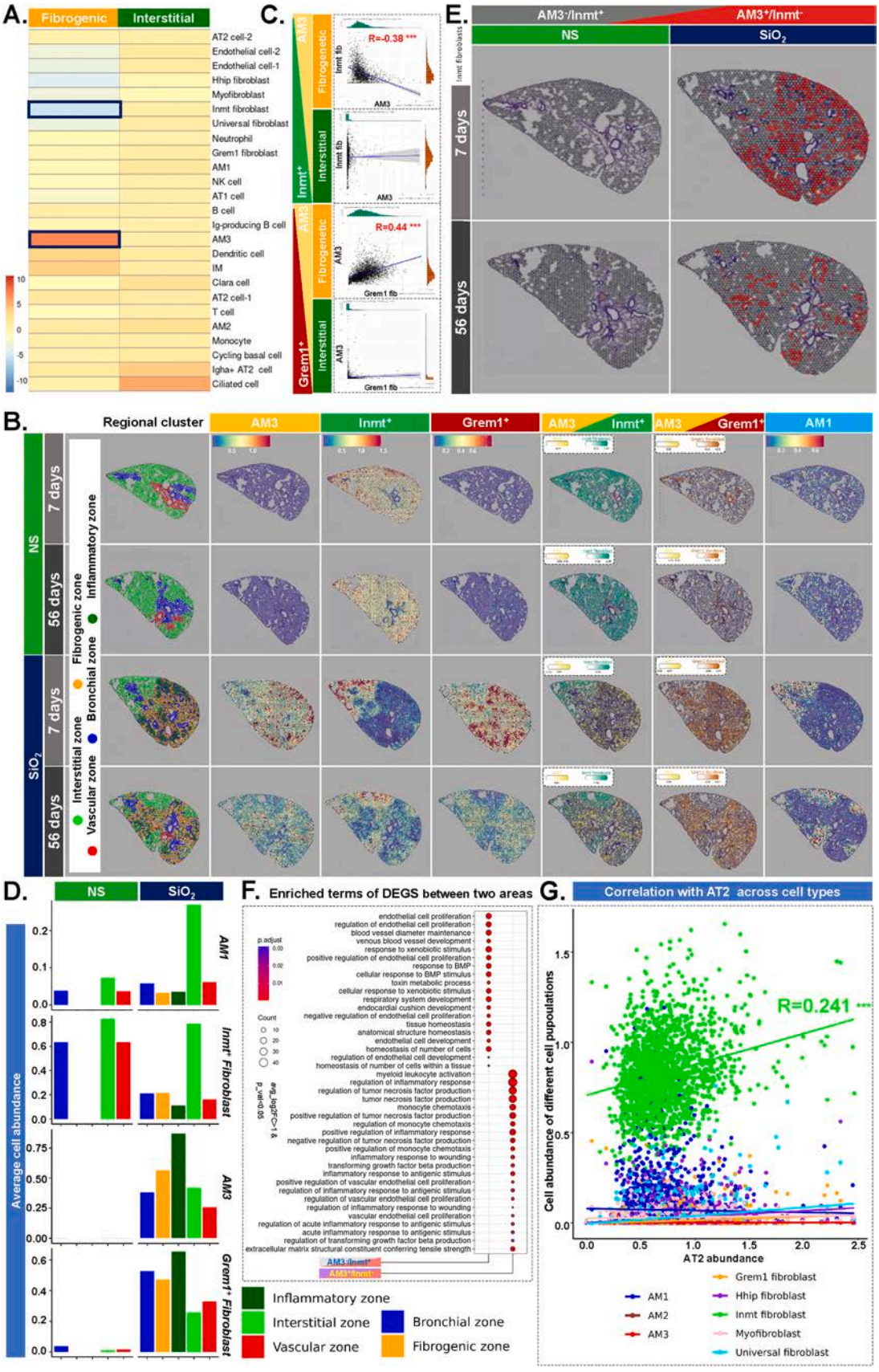

(caption on next page)

Fig. 7. Silica particles sculpted a fibrotic microenvironment. (A) MIA showed the enrichment map of all scRNA-seq-identified cell types in fibrogenic and inflammatory regions. Red indicates enrichment (significantly high overlap); blue indicates depletion (significantly low overlap). **(B)** The first column show the five defined regions (the same as in Fig. 6C for the readership) and the other columns show the cell abundance of AM3 macrophages and Inmt fibroblasts as well as AM1 macrophages and Grem1 fibroblasts, or the combination of different cell abundance. **(C)** The upper scatter plot show the correlation between AM3 macrophages and Inmt fibroblasts in the same spot from interstitial or fibrogenic region;the lower scatter plot show the correlation between AM3 macrophages and Grem1 fibroblasts in the same spot from interstitial or fibrogenic region. **(D)** The boxplot shows average cell abundance of different conditions across defined five regions. To better present and interpret the results, we combined NS_7 and NS_56 into a single NS group, and SiO_2_7 and SiO_2_56 into a single SiO_2 group for the cell proportion analysis. All the missing time points are included in the Fig. S7E-H. **(E)** The spatial slides highlight spots with AM3 macrophages but lacking Inmt fibroblasts ($AM3^+Inmt^-$) in red, and spots with Inmt fibroblasts but lacking AM3 macrophages ($AM3^-Inmt^+$) in grey. **(F)** Enriched GO terms for the degs between $AM3^+$ $Inmt^-$ and $AM3^-$ $Inmt^+$ spots from fibrogenic, inflammatory and interstitial zone. **(G)** A scatter plot illustrates the relationship between AM1, AM2, AM3, Grem1, Hhip, Inmt, universal fibroblast, and myofibroblast with AT2.

disease progression. We utilized a spatially resolved transcriptome technique to map the transcriptional changes during lung injury and identify genetic alterations in the lesion region. Our spatial transcriptome sequencing results revealed that lung tissue can be divided into five regions. Notably, in the lung interstitial zone, excluding the bronchial and vascular zones, SiO_2 stimulation resulted in the formation of inflammatory and fibrogenic zones. However, these damaged areas did not exhibit the same pattern of periphery-to-center progression seen in mechanical tension-induced pulmonary fibrosis or IPF of unknown etiology [76]. Further investigation of the spatial distribution of fibroblast subtypes and alveolar macrophage subtypes in the mechanical tension-induced pulmonary fibrosis model could enhance our understanding of the differences between different causes of pulmonary fibrosis. In this study, we found that Inmt fibroblasts with tissue homeostasis functions co-localized with AM1 macrophages, while pro-fibrotic AM3 macrophages co-localized with Grem1 fibroblasts. The spatial misalignment of Inmt fibroblasts and AM3 macrophages suggests abnormal crosstalk between Inmt fibroblasts and AM3 macrophages in silicosis. However, the specific molecular mechanisms underlying this process remain to be elucidated.

5. Conclusion

In this study, we explored the heterogeneity in pathological alterations within tissues of lung fibrosis, attributing the observed variability to differential timing and spatial distribution of pathophysiological events. Employing spatial transcriptomics, we achieved a nuanced understanding of the microenvironmental dynamics and intercellular communications within fibrotic regions of the lung. This advanced approach facilitated the identification of distinctive gene expression patterns, elucidating alterations in cell populations pivotal for homeostasis and pathology. Specifically, we found a subset of fibroblasts, called Inmt fibroblasts, exerted a suppressive role in the fibrotic microenvironment. Our analysis revealed an increase in AM3 macrophages and Grem1 fibroblasts, alongside a reduction in Inmt fibroblasts and AM1 macrophages distributed throughout fibrotic lung areas. We validated that monocyte-derived AM3 could decrease Inmt fibroblast populations and increase Grem1 fibroblast numbers, potentially disrupting lung homeostasis in response to external challenges. Furthermore, our findings highlighted the central role of fibroblast-macrophage interactions in the fibrotic process, suggesting a complex network of cellular compartments orchestrating fibrosis development and aberrant tissue responses.

Study approval

We used the gene expression in pulmonary fibrosis tissue and clinical data included in the GSE135893 dataset, consisting of 10 controls and 12 IPF cases [43]. For both IPF and control lungs, tissue sampling was performed in two centers (VUMC and NTI) at the time of lung transplantation. Ethical approval was granted at the time of the initial study [43]. This work has received approval for research ethics from the Laboratory Animal Care and Use Committee of Southeast University and a proof/certificate of approval is available upon request. All animal experiments were approved by the Laboratory Animal Care and Use Committee of Southeast University (20190121002).

Environmental implication

As crystalline silica is widely encountered in numerous industrial occupations and even in everyday life. Irreversible silicosis caused by crystalline silica particles represent significant global disease burden. This study elucidated how the fibrotic microenvironment is spatially organized in lung fibrosis induced by silica particles. In particular, we confirmed that monocyte-derived alveolar macrophages (AM3) can help Inmt fibroblasts shift into the profibrotic Grem1 fibroblasts. Our findings underscore the need for more effective methods to silica safety management and provide a possible avenue for minimizing silica-related lung damage.

List of abbreviations

List of abbreviations.

AM	Alveolar macrophage
AM3	alveolar macrophage subset cluster 3
IM	Interstitial macrophage
UMAP	Uniform Manifold Approximation and Projection
LASSO	Least Absolute Shrinkage and Selection Operator
IPF	Idiopathic pulmonary fibrosis
PCA	Principal component analysis
scRNA-seq	single-cell RNA sequencing
ST	Spatial transcriptomics
NS	Normal saline
SiO_2	Silicon dioxide(Silica particles)
CCR2	C–C chemokine receptor 2
MIA	multimodal intersection analysis

Compliance and ethics

Liliang Yang declares that he does not have any Conflict of Interest.
Xinyan Wei declares that she does not have any Conflict of Interest.
Piaopiao Sun declares that he does not have any Conflict of Interest.
Xinbei Zhou declares that she does not have any Conflict of Interest.
Xinxin Zhang declares that she does not have any Conflict of Interest.
Wei Luo declares that she does not have any Conflict of Interest.
Yun Zhou declares that she does not have any Conflict of Interest.
Wei Zhang declares that she does not have any Conflict of Interest.
Shencun Fang declares that she does not have any Conflict of Interest.
Jie Chao declares that he does not have any Conflict of Interest.

Funding

This work was supported by National Key R&D Program of China (2022YFC2504403); the National Natural Science Foundation of China grant (82373547, 81972987, 81773796, and 81700068, 81803182); the Natural Science Foundation of Jiangsu Province, China (No. BK20221184); the Jiangsu Provincial Key Laboratory of Critical Care

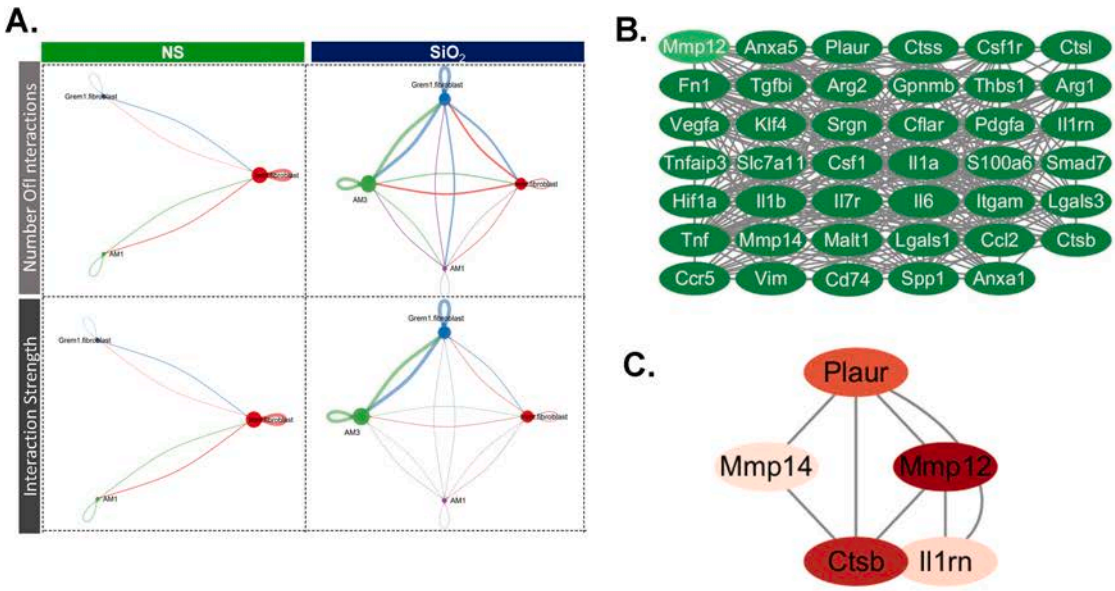

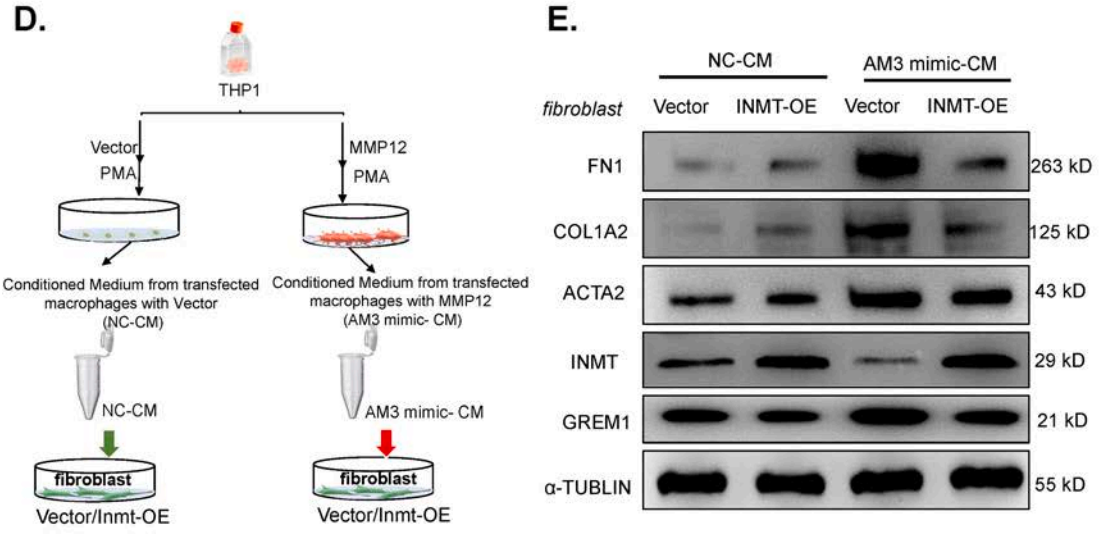

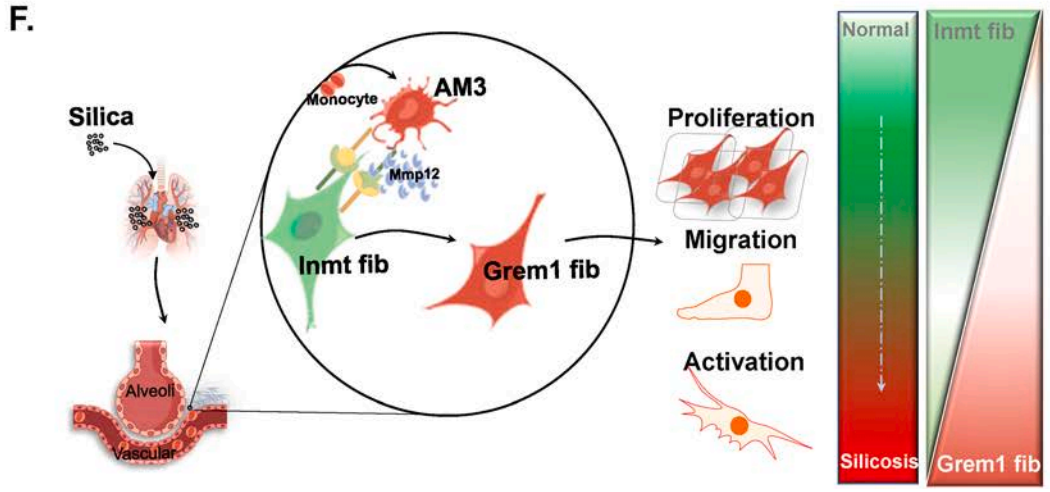

(caption on next page)

Fig. 8. AM3 macrophages induce Inmt fibroblast transdifferentiation into Grem1 fibroblasts. (A) Cell-cell interactions in ST were performed using cellchat2**.** Since SiO_2_7 and SiO_2_56 have similar spot signatures (Fig. 6B,first column), and NS_7 and NS_56 also share similar spot signatures (Fig. 6B,first column), we combined SiO_2_7 and SiO_2_56 into a single SiO_2 group, and NS_7 and NS_56 into a single NS group, thereby enhancing the statistical significance of the data. We then performed cell communication analysis on the cellular subtypes within the NS and SiO_2 groups. **(B)** Cytoscape visualizes protein-protein interaction (PPI) analysis on fibrosis-related genes in AM3**. (C)** "MCODE" algorithm in Cytoscape software was used to identify key clustering modules, with MMP12 identified as the module core. **(D)** The process of obtaining macrophage conditioned culture medium (CM) for coculture with fibroblasts**. (E)** Overexpression of *INMT* partially reversed the AM3 mimic-CM induced increase in the expression of FN1, COL1A2, ACTA2 and GREM1.**(F)** Effects of monocyte-derived AM3 macrophages on fibroblasts function and mechanisms in the silicosis process.

Medicine grant (JSKLCCM-2022-02-005); the Fundamental Research Funds for the Central Universities (2242023K40004).

CRediT authorship contribution statement

Wei Luo: Visualization, Methodology. **Wei Zhang:** Writing – review & editing, Visualization. **Yun Zhou:** Visualization, Methodology. **Jie Chao:** Writing – review & editing, Writing – original draft, Supervision, Resources, Project administration, Investigation, Funding acquisition, Conceptualization. **Shencun Fang:** Writing – review & editing, Writing – original draft, Supervision, Funding acquisition, Conceptualization. **Xinyan Wei:** Writing – review & editing, Visualization, Validation, Methodology, Formal analysis. **Liliang Yang:** Writing – review & editing, Writing – original draft, Visualization, Validation, Software, Methodology, Investigation, Formal analysis, Data curation, Conceptualization. **Jing Wang:** Writing – review & editing, Methodology, Formal analysis. **Piaopiao Sun:** Writing – review & editing, Visualization, Methodology, Data curation. **Xinxin Zhang:** Visualization, Methodology. **Xinbei Zhou:** Software, Methodology, Formal analysis.

Declaration of Competing Interest

The authors declare that they have no known competing financial interests or personal relationships that could have appeared to influence the work reported in this paper.

Data Availability

Data will be made available on request.

Acknowledgments

We thank LetPub (www.letpub.com) for linguistic assistance and pre-submission expert review. This research work is supported by the Big Data Computing Center of Southeast University. We thank Professor Wei Jiang for the valuable constructive criticism.We thank Dr. Jianming Zeng and his bioinformatics team for their reference codes.

Appendix A. Supporting information

Supplementary data associated with this article can be found in the online version at doi:10.1016/j.jhazmat.2024.135540.

References

[1] Hoy, R.F., Jeebhay, M.F., Cavalin, C., Chen, W., Cohen, R.A., Fireman, E., et al., 2022. Current global perspectives on silicosis-Convergence of old and newly emergent hazards. Respirology 27, 387–398.
[2] Lurje, I., Gaisa, N.T., Weiskirchen, R., Tacke, F., 2023. Mechanisms of organ fibrosis: emerging concepts and implications for novel treatment strategies. Mol Asp Med 92, 101191.
[3] Zhang, X., Shi, X., Xie, F., Liu, Y., Wei, X., Cai, Y., et al., 2023. Dissecting pulmonary fibroblasts heterogeneity in lung development, health and diseases. Heliyon 9, e19428.
[4] Lendahl, U., Muhl, L., Betsholtz, C., 2022. Identification, discrimination and heterogeneity of fibroblasts. Nat Commun 13, 3409.
[5] Gu, Y., Lawrence, T., Mohamed, R., Liang, Y., Yahaya, B.H., 2022. The emerging roles of interstitial macrophages in pulmonary fibrosis: a perspective from scRNA-seq analyses. Front Immunol 13, 923235.
[6] Uderhardt, S., Martins, A.J., Tsang, J.S., Lammermann, T., Germain, R.N., 2019. Resident macrophages cloak tissue microlesions to prevent neutrophil-driven inflammatory damage. Cell 177, 541–555 e517.
[7] Mossadegh-Keller, N., Sarrazin, S., Kandalla, P.K., Espinosa, L., Stanley, E.R., Nutt, S.L., et al., 2013. M-CSF instructs myeloid lineage fate in single haematopoietic stem cells. Nature 497, 239–243.
[8] Duffield, J.S., Forbes, S.J., Constandinou, C.M., Clay, S., Partolina, M., Vuthoori, S., et al., 2005. Selective depletion of macrophages reveals distinct, opposing roles during liver injury and repair. J Clin Invest 115, 56–65.
[9] Xie, T., Wang, Y., Deng, N., Huang, G., Taghavifar, F., Geng, Y., et al., 2018. Single-cell deconvolution of fibroblast heterogeneity in mouse pulmonary fibrosis. Cell Rep 22, 3625–3640.
[10] Hussell, T., Bell, T.J., 2014. Alveolar macrophages: plasticity in a tissue-specific context. Nat Rev Immunol 14, 81–93.
[11] Bian, Z.L., Gong, Y.D., Huang, T., Lee, C.Z.W., Bian, L.H., Bai, Z.J., et al., 2020. Deciphering human macrophage development at single-cell resolution. Nature 582, 571–576.
[12] Chakarov, S., Lim, H.Y., Tan, L., Lim, S.Y., See, P., Lum, J., et al., 2019. Two distinct interstitial macrophage populations coexist across tissues in specific subtissular niches. Science 363, eaau0964.
[13] Mari, B., Crestani, B., 2019. Dysregulated balance of lung macrophage populations in idiopathic pulmonary fibrosis revealed by single-cell RNA seq: an unstable "ménage-à-trois. Eur Respir J 54, 1901229.
[14] Wendisch, D., Dietrich, O., Mari, T., von Stillfried, S., Ibarra, I.L., Mittermaier, M., et al., 2021. SARS-CoV-2 infection triggers profibrotic macrophage responses and lung fibrosis. Cell 184, 6243–6261 e6227.
[15] Fastrès, A., Pirottin, D., Fievez, L., Tutunaru, A.-C., Bolen, G., Merveille, A.-C., et al., 2020. Identification of pro-fibrotic macrophage populations by single-cell transcriptomic analysis in west highland white terriers affected with canine idiopathic pulmonary fibrosis. Front Immunol 11, 611749.
[16] Martinet, Y., Rom, W.N., Grotendorst, G.R., Martin, G.R., Crystal, R.G., 1987. Exaggerated spontaneous release of platelet-derived growth factor by alveolar macrophages from patients with idiopathic pulmonary fibrosis. N Engl J Med 317, 202–209.
[17] Eyres, M., Bell, J.A., Davies, E.R., Fabre, A., Alzetani, A., Jogai, S., et al., 2022. Spatially resolved deconvolution of the fibrotic niche in lung fibrosis. Cell Rep 40, 111230.
[18] Stahl, P.L., Salmen, F., Vickovic, S., Lundmark, A., Navarro, J.F., Magnusson, J., et al., 2016. Visualization and analysis of gene expression in tissue sections by spatial transcriptomics. Science 353, 78–82.
[19] Wang, S., Luo, W., Huang, J., Chen, M.L., Ding, J.W., Cheng, Y.S., et al., 2022. The combined effects of circular RNA methylation promote pulmonary fibrosis. Am J Respir Cell Mol Biol 66, 510–523.
[20] Chen, M., Wang, J., Yuan, M., Long, M., Sun, Y., Wang, S., et al., 2023. AT2 cell-derived IgA trapped by the extracellular matrix in silica-induced pulmonary fibrosis. Int Immunopharmacol 122, 110545.
[21] Trapnell, C., Cacchiarelli, D., Grimsby, J., Pokharel, P., Li, S., Morse, M., et al., 2014. The dynamics and regulators of cell fate decisions are revealed by pseudotemporal ordering of single cells. Nat Biotechnol 32, 381–386.
[22] Abd ElHafeez, S., D'Arrigo, G., Leonardis, D., Fusaro, M., Tripepi, G., Roumeliotis, S., 2021. Methods to analyze time-to-event data: The cox regression analysis. Oxid Med Cell Longev 2021, 1302811.
[23] Friedman, J., Hastie, T., Tibshirani, R., 2010. Regularization paths for generalized linear models via coordinate descent. J Stat Softw 33, 1–22.
[24] Kleshchevnikov, V., Shmatko, A., Dann, E., Aivazidis, A., King, H.W., Li, T., et al., 2022. Cell2location maps fine-grained cell types in spatial transcriptomics. Nat Biotechnol 40, 661–671.
[25] Jin, S.Q., Guerrero-Juarez, C.F., Zhang, L.H., Chang, I., Ramos, R., Kuan, C.H., et al., 2021. Inference and analysis of cell-cell communication using CellChat. Nat Commun 12, 1088.
[26] Shi, X., Wang, J., Zhang, X., Yang, S., Luo, W., Wang, S., et al., 2022. GREM1/PPP2R3A expression in heterogeneous fibroblasts initiates pulmonary fibrosis. Cell Biosci 12, 123.
[27] Jin, S., Guerrero-Juarez, C.F., Zhang, L., Chang, I., Ramos, R., Kuan, C.H., et al., 2021. Inference and analysis of cell-cell communication using CellChat. Nat Commun 12, 1088.
[28] Morse, C., Tabib, T., Sembrat, J., Buschur, K.L., Bittar, H.T., Valenzi, E., et al., 2019. Proliferating SPP1/MERTK-expressing macrophages in idiopathic pulmonary fibrosis. Eur Respir J 54.
[29] Cui, H., Jiang, D., Banerjee, S., Xie, N., Kulkarni, T., Liu, R.M., et al., 2020. Monocyte-derived alveolar macrophage apolipoprotein E participates in pulmonary fibrosis resolution. Jci Insight 5.

[30] Shi, X., Chen, Y., Shi, M., Gao, F., Huang, L., Wang, W., et al., 2024. The novel molecular mechanism of pulmonary fibrosis: insight into lipid metabolism from reanalysis of single-cell RNA-seq databases. Lipids Health Dis 23, 98.
[31] Hallahan, D.E., Geng, L., Shyr, Y., 2002. Effects of intercellular adhesion molecule 1 (ICAM-1) null mutation on radiation-induced pulmonary fibrosis and respiratory insufficiency in mice. J Natl Cancer Inst 94, 733–741.
[32] Radwanska, A., Cottage, C.T., Piras, A., Overed-Sayer, C., Sihlbom, C., Budida, R., et al., 2022. Increased expression and accumulation of GDF15 in IPF extracellular matrix contribute to fibrosis. Jci Insight 7.
[33] Yang, L., Zhou, F., Zheng, D., Wang, D., Li, X., Zhao, C., et al., 2021. FGF/FGFR signaling: from lung development to respiratory diseases. Cytokine Growth Factor Rev 62, 94–104.
[34] Zhou, B.W., Liu, H.M., Xu, F., Jia, X.H., 2024. The role of macrophage polarization and cellular crosstalk in the pulmonary fibrotic microenvironment: a review. Cell Commun Signal 22, 172.
[35] Dubey, S., Dubey, P.K., Umeshappa, C.S., Ghebre, Y.T., Krishnamurthy, P., 2022. Inhibition of RUNX1 blocks the differentiation of lung fibroblasts to myofibroblasts. J Cell Physiol 237, 2169–2182.
[36] Schubert, M., Klinger, B., Klunemann, M., Sieber, A., Uhlitz, F., Sauer, S., et al., 2018. Perturbation-response genes reveal signaling footprints in cancer gene expression. Nat Commun 9, 20.
[37] Qiu, X., Mao, Q., Tang, Y., Wang, L., Chawla, R., Pliner, H.A., et al., 2017. Reversed graph embedding resolves complex single-cell trajectories. Nat Methods 14, 979–982.
[38] Wang, J.F., Wang, Y.T., Bi, J.B., 2022. Indolethylamine-N-methyltransferase inhibits proliferation and promotes apoptosis of human prostate cancer cells: a mechanistic exploration. Front Cell Dev Biol 10.
[39] Liu, X., Rowan, S.C., Liang, J., Yao, C., Huang, G., Deng, N., et al., 2021. Categorization of lung mesenchymal cells in development and fibrosis. iScience 24, 102551.
[40] Ogawa, T., Shichino, S., Ueha, S., Bando, K., Matsushima, K., 2022. Profibrotic properties of C1q(+) interstitial macrophages in silica-induced pulmonary fibrosis in mice. Biochem Biophys Res Commun 599, 113–119.
[41] Davis, A.P., Grondin, C.J., Johnson, R.J., Sciaky, D., King, B.L., McMorran, R., et al., 2017. The comparative toxicogenomics database: Update 2017. Nucleic Acids Res 45, D972–D978.
[42] Xie, T., Wang, Y.Z., Deng, N., Huang, G.L., Taghavifar, F., Geng, Y., et al., 2018. Single-cell deconvolution of fibroblast heterogeneity in mouse pulmonary fibrosis. Cell Rep 22, 3625–3640.
[43] Habermann, A.C., Gutierrez, A.J., Bui, L.T., Yahn, S.L., Winters, N.I., Calvi, C.L., et al., 2020. Single-cell RNA sequencing reveals profibrotic roles of distinct epithelial and mesenchymal lineages in pulmonary fibrosis. Sci Adv 6, eaba1972.
[44] Sauter, K.A., Pridans, C., Sehgal, A., Tsai, Y.T., Bradford, B.M., Raza, S., et al., 2014. Pleiotropic effects of extended blockade of CSF1R signaling in adult mice. J Leukoc Biol 96, 265–274.
[45] Shibata, Y., Zsengeller, Z., Otake, K., Palaniyar, N., Trapnell, B.C., 2001. Alveolar macrophage deficiency in osteopetrotic mice deficient in macrophage colony-stimulating factor is spontaneously corrected with age and associated with matrix metalloproteinase expression and emphysema. Blood 98, 2845–2852.
[46] Misharin, A.V., Morales-Nebreda, L., Reyfman, P.A., Cuda, C.M., Walter, J.M., McQuattie-Pimentel, A.C., et al., 2017. Monocyte-derived alveolar macrophages drive lung fibrosis and persist in the lung over the life span. J Exp Med 214, 2387–2402.
[47] Habermann, A.C., Gutierrez, A.J., Bui, L.T., Yahn, S.L., Winters, N.I., Calvi, C.L., et al., 2020. Single-cell RNA sequencing reveals profibrotic roles of distinct epithelial and mesenchymal lineages in pulmonary fibrosis. Sci Adv 6, eaba1972.
[48] Moncada, R., Barkley, D., Wagner, F., Chiodin, M., Devlin, J.C., Baron, M., et al., 2020. Integrating microarray-based spatial transcriptomics and single-cell RNA-seq reveals tissue architecture in pancreatic ductal adenocarcinomas. Nat Biotechnol 38, 333–342.
[49] Olajuyin, A.M., Zhang, X., Ji, H.L., 2019. Alveolar type 2 progenitor cells for lung injury repair. Cell Death Discov 5, 63.
[50] Mayr, C.H., Sengupta, A., Asgharpour, S., Ansari, M., Pestoni, J.C., Ogar, P., et al., 2024. Sfrp1 inhibits lung fibroblast invasion during transition to injury-induced myofibroblasts. Eur Respir J 63.
[51] Qi, J., Sun, H., Zhang, Y., Wang, Z., Xun, Z., Li, Z., et al., 2022. Single-cell and spatial analysis reveal interaction of FAP(+) fibroblasts and SPP1(+) macrophages in colorectal cancer. Nat Commun 13, 1742.
[52] Buechler, M.B., Pradhan, R.N., Krishnamurty, A.T., Cox, C., Calviello, A.K., Wang, A.W., et al., 2021. Cross-tissue organization of the fibroblast lineage. Nature 593, 575–579.
[53] Jianfeng, W., Yutao, W., Jianbin, B., 2022. Indolethylamine-N-Methyltransferase Inhibits Proliferation and Promotes Apoptosis of Human Prostate Cancer Cells: A Mechanistic Exploration. Front Cell Dev Biol 10, 805402.
[54] Tsukui, T., Sun, K.H., Wetter, J.B., Wilson-Kanamori, J.R., Hazelwood, L.A., Henderson, N.C., et al., 2020. Collagen-producing lung cell atlas identifies multiple subsets with distinct localization and relevance to fibrosis. Nat Commun 11, 1920.
[55] Mills, C.D., Kincaid, K., Alt, J.M., Heilman, M.J., Hill, A.M., 2000. M-1/M-2 macrophages and the Th1/Th2 paradigm. J Immunol 164, 6166–6173.
[56] Joshi, N., Watanabe, S., Verma, R., Jablonski, R.P., Chen, C.I., Cheresh, P., et al., 2020. A spatially restricted fibrotic niche in pulmonary fibrosis is sustained by M-CSF/M-CSFR signalling in monocyte-derived alveolar macrophages. Eur Respir J 55.
[57] Xie, T., Kulur, V., Liu, N., Deng, N., Wang, Y., Rowan, S.C., et al., 2021. Mesenchymal growth hormone receptor deficiency leads to failure of alveolar progenitor cell function and severe pulmonary fibrosis. Sci Adv 7.
[58] Wendisch, D., Dietrich, O., Mari, T., von Stillfried, S., Ibarra, I.L., Mittermaier, M., et al., 2021. SARS-CoV-2 infection triggers profibrotic macrophage responses and lung fibrosis. Cell 184, 6243–6261 e6227.
[59] Gosselin, D., Link, V.M., Romanoski, C.E., Fonseca, G.J., Eichenfield, D.Z., Spann, N.J., et al., 2014. Environment drives selection and function of enhancers controlling tissue-specific macrophage identities. Cell 159, 1327–1340.
[60] Gautier, E.L., Shay, T., Miller, J., Greter, M., Jakubzick, C., Ivanov, S., et al., 2012. C. Immunological Genome, Gene-expression profiles and transcriptional regulatory pathways that underlie the identity and diversity of mouse tissue macrophages. Nat Immunol 13, 1118–1128.
[61] Garrido-Trigo, A., Corraliza, A.M., Veny, M., Dotti, I., Melon-Ardanaz, E., Rill, A., et al., 2023. Macrophage and neutrophil heterogeneity at single-cell spatial resolution in human inflammatory bowel disease. Nat Commun 14, 4506.
[62] Matusiak, M., Hickey, J.W., van, I.D.G.P., Lu, G., Kidzinski, L., Zhu, S., et al., 2024. Spatially segregated macrophage populations predict distinct outcomes in colon. Cancer, Cancer Discov.
[63] Viola, M.F., Boeckxstaens, G., 2021. Niche-specific functional heterogeneity of intestinal resident macrophages. Gut 70, 1383–1395.
[64] Heinrich, S., Craig, A.J., Ma, L.C., Heinrich, B., Greten, T.F., Wang, X.W., 2021. Understanding tumour cell heterogeneity and its implication for immunotherapy in liver cancer using single-cell analysis. J Hepatol 74, 700–715.
[65] Vallejo, J., Cochain, C., Zernecke, A., Ley, K., 2021. Heterogeneity of immune cells in human atherosclerosis revealed by scRNA-Seq. Cardiovasc Res 117, 2537–2543.
[66] Morse, C., Tabib, T., Sembrat, J., Buschur, K.L., Bittar, H.T., Valenzi, E., et al., 2019. Proliferating SPP1/MERTK-expressing macrophages in idiopathic pulmonary fibrosis. Eur Respir J 54, 1802441.
[67] Ramachandran, P., Pellicoro, A., Vernon, M.A., Boulter, L., Aucott, R.L., Ali, A., et al., 2012. Differential Ly-6C expression identifies the recruited macrophage phenotype, which orchestrates the regression of murine liver fibrosis. Proc Natl Acad Sci USA 109, E3186–E3195.
[68] Psarras, S., Mavroidis, M., Sanoudou, D., Davos, C.H., Xanthou, G., Varela, A.E., et al., 2011. Regulation of adverse remodelling by osteopontin in a genetic heart failure model. Eur Heart J 33, 1954–1963.
[69] Hohensinner, P.J., Baumgartner, J., Kral-Pointner, J.B., Uhrin, P., Ebenbauer, B., Thaler, B., et al., 2017. Activator Inhibitor-1) expression renders alternatively activated human macrophages proteolytically quiescent. Arterioscler, Thromb, Vasc Biol 37, 1913–1922.
[70] Buechler, M.B., Fu, W., Turley, S.J., 2021. Fibroblast-macrophage reciprocal interactions in health, fibrosis, and cancer. Immunity 54, 903–915.
[71] Morrone, C., Smirnova, N.F., Jeridi, A., Kneidinger, N., Hollauer, C., Schupp, J.C., et al., 2020. Cathepsin B promotes collagen biosynthesis, which drives bronchiolitis obliterans syndrome. Eur Respir J 57, 2001416.
[72] Zhang, S.Y., Wan, D., Zhu, M.C., Wang, G.H., Zhang, X.R., Huang, N., et al., 2022. $CD11b^{+}CD43^{hi}Ly6C^{lo}$ splenocyte-derived macrophages exacerbate liver fibrosis via spleen–liver axis (in-press). Hepatology 1–18.
[73] Sveiven, S.N., Nordgren, T.M., 2020. Lung-resident mesenchymal stromal cells are tissue-specific regulators of lung homeostasis. Am J Physiol Lung Cell Mol Physiol 319, L197–L210.
[74] Davidson, S., Coles, M., Thomas, T., Kollias, G., Ludewig, B., Turley, S., et al., 2021. Fibroblasts as immune regulators in infection, inflammation and cancer. Nat Rev Immunol 21, 704–717.
[75] You, Y., Yuan, H., Min, H., Li, C., Chen, J., 2023. Fibroblast-derived CXCL14 aggravates crystalline silica-induced pulmonary fibrosis by mediating polarization and recruitment of interstitial macrophages. J Hazard Mater 460, 132489.
[76] Wu, H., Yu, Y., Huang, H., Hu, Y., Fu, S., Wang, Z., et al., 2020. Progressive pulmonary fibrosis is caused by elevated mechanical tension on alveolar stem cells. Cell 180, 107–121 e117.